



Environmental changes during the onset of the Late Pliensbachian Event (Early Jurassic) in the Cardigan Bay Basin, Wales

Teuntje P. Hollaar^{1,2}, Stephen P. Hesselbo^{2,3}, Jean-François Deconinck⁴, Magret Damaschke⁵, Clemens V. Ullmann^{2,3}, Mengjie Jiang², and Claire M. Belcher¹

¹WildFIRE Lab, Global Systems Institute, University of Exeter, Exeter, EX4 4PS, UK

²Camborne School of Mines, Department of Earth and Environmental Sciences, University of Exeter, Penryn Campus, Penryn, TR10 9FE, UK

³Environment and Sustainability Institute, University of Exeter, Penryn Campus, Penryn, TR10 9FE, UK

⁴Biogéosciences, UMR 6282 CNRS, Université de Bourgogne/Franche-Comté, 21000 Dijon, France

⁵Core Scanning Facility, British Geological Survey, Keyworth, NG12 5GG, UK

Correspondence: Teuntje P. Hollaar (t.p.hollaar@exeter.ac.uk)

Received: 8 November 2022 – Discussion started: 30 November 2022

Revised: 24 March 2023 – Accepted: 7 April 2023 – Published: 15 May 2023

Abstract. The Late Pliensbachian Event (LPE), in the Early Jurassic, is associated with a perturbation in the global carbon cycle (positive carbon isotope excursion (CIE) of $\sim 2\%$), cooling of $\sim 5^\circ\text{C}$, and the deposition of widespread regressive facies. Cooling during the late Pliensbachian has been linked to enhanced organic matter burial and/or disruption of thermohaline ocean circulation due to a sea level lowstand of at least regional extent. Orbital forcing had a strong influence on the Pliensbachian environments and recent studies show that the terrestrial realm and the marine realm in and around the Cardigan Bay Basin, UK, were strongly influenced by orbital climate forcing. In the present study we build on the previously published data for long eccentricity cycle $E459 \pm 1$ and extend the palaeoenvironmental record to include $E458 \pm 1$. We explore the environmental and depositional changes on orbital timescales for the Llanbedr (Mochras Farm) core during the onset of the LPE. Clay mineralogy, X-ray fluorescence (XRF) elemental analysis, isotope ratio mass spectrometry, and palynology are combined to resolve systematic changes in erosion, weathering, fire, grain size, and riverine influx. Our results indicate distinctively different environments before and after the onset of the LPE positive CIE and show increased physical erosion relative to chemical weathering. We also identify five swings in the climate, in tandem with the 405 kyr eccentricity minima

and maxima. Eccentricity maxima are linked to precessionally repeated occurrences of a semi-arid monsoonal climate with high fire activity and relatively coarser sediment from terrestrial runoff. In contrast, 405 kyr minima in the Mochras core are linked to a more persistent, annually wet climate, low fire activity, and relatively finer-grained deposits across multiple precession cycles. The onset of the LPE positive CIE did not impact the expression of the 405 kyr cycle in the proxy records; however, during the second pulse of heavier carbon (^{13}C) enrichment, the clay minerals record a change from dominant chemical weathering to dominant physical erosion.

1 Introduction

The Early Jurassic is a period marked by large climatic fluctuations and associated carbon isotope excursions (CIEs) in an overall warmer than present and high- $p\text{CO}_2$ world (McElwain et al., 2005; Korte and Hesselbo, 2011; Steinthorsdottir and Vajda, 2015; Korte et al., 2015; Robinson et al., 2016). A series of small and medium-sized CIEs have recently been documented for the Sinemurian and Pliensbachian, which have mainly been from European, North African, and North American records (Korte and Hesselbo, 2011; Franceschi et

al., 2014; Korte et al., 2015; Price et al., 2016; De Lena et al., 2019; Hesselbo et al., 2020a; Mercuzot et al., 2020; Storm et al., 2020; Silva et al., 2021; Cifer et al., 2022; Bodin et al., 2023). Notable is the pronounced positive CIE in the late Pliensbachian, which has been called the Late Pliensbachian Event (LPE) and is linked to climatic cooling (Hesselbo and Korte, 2011; Korte et al., 2015) and a supra-regional/global sea level lowstand (Hallam, 1981; de Graciansky et al., 1998; Hesselbo and Jenkyns, 1998; Hesselbo, 2008). The LPE has been recognized by a positive shift in benthic marine oxygen isotopes ($\sim 1.5\text{‰}$ – 2‰) (Bailey et al., 2003; Rosales et al., 2004, 2006; Suan et al., 2010; Dera et al., 2011a; Korte and Hesselbo, 2011; Gómez et al., 2016; Alberti et al., 2019, 2021), coeval with a positive shift in marine and terrestrial carbon isotopes ($\sim 2\text{‰}$) (Jenkyns and Clayton, 1986; McArthur et al., 2000; Morettini et al., 2002; Quesada et al., 2005; Rosales et al., 2006; Suan et al., 2010; Korte and Hesselbo, 2011; Silva et al., 2011; Gómez et al., 2016; De Lena et al., 2019).

A cooler late Pliensbachian climate has been suggested based on low $p\text{CO}_2$ values inferred by leaf stomatal index data from eastern Australia (Steinhorsdottir and Vajda, 2015), the presence of glendonites in northern Siberia (Kaplan, 1978; Price, 1999; Rogov and Zakharov, 2010), vegetation shifts from a diverse flora of different plant groups to one mainly dominated by bryophytes in Siberia (Ilyina, 1985; Zakharov et al., 2006), and possible ice-rafted debris found in Siberia (Price, 1999; Suan et al., 2011). Whilst the presence of ice sheets is strongly debated, a general cooling period ($\sim 5^\circ\text{C}$ lower; Korte et al., 2015; Gómez et al., 2016) is evident from several temperature reconstructions from NW Europe. A cooling is hypothesized via enhanced carbon burial in the marine sediments, leading to lower $p\text{CO}_2$ values and initiating cooler climatic conditions (Jenkyns and Clayton, 1986; Suan et al., 2010; Silva et al., 2011; Storm et al., 2020). Direct evidence of large-scale carbon burial in upper Pliensbachian marine deposits has not yet been documented (Silva et al., 2021). Alternatively, cooling has been suggested to be caused by a lower sea level which would have disrupted ocean circulation in the Laurasian Seaway, reducing poleward heat transport from the tropics (Korte et al., 2015). In the UK region, a dome structure in the North Sea has been linked to the shedding of sediments during sea level lowstands from the late Toarcian and possibly before (Underhill and Partington, 1993; Korte et al., 2015; Archer et al., 2019). Disruption of the ocean circulation between the western Tethys and the Boreal realm is supported by marine migration patterns (Schweigert, 2005; Zakharov et al., 2006; Bourillot et al., 2008; Nikitenko, 2008; Dera et al., 2011; van de Schootbrugge et al., 2019) and numerical models (Bjerrum et al., 2001; Dera and Donnadieu, 2012; Ruvalcaba Baroni et al., 2018); however, the net direction of the flows remains debated.

An additional factor to be considered is that a strong orbital control exists on the Pliensbachian sedimentary succes-

sions (Weedon and Jenkyns, 1990; Ruhl et al., 2016; Hinov et al., 2018; Storm et al., 2020; Hollaar et al., 2021). Previous studies have indicated that sea level changes, possibly coupled to glacioeustatic rise and fall, occurred during the LPE on a 100 kyr (short eccentricity) timescale (Korte and Hesselbo, 2011). A high-resolution record of charcoal, clay mineralogy, bulk-organic carbon isotopes, total organic carbon (TOC), and CaCO_3 encompassing approximately one 405 kyr cycle from the Llanbedr (Mochras Farm) borehole, Cardigan Bay Basin, NW Wales, UK, suggested that the long eccentricity orbital cycle had a significant effect on background climatic and environmental change during the late Pliensbachian, particularly affecting the hydrological regime of the region (Hollaar et al., 2021). This previous research focussed on orbital forcing of environmental change for a time lacking any large excursion in $\delta^{13}\text{C}_{\text{org}}$ and so unaffected by perturbations to the global carbon cycle. Here, we expand on the record of Hollaar et al. (2021) to cover two long eccentricity cycles (which we identify as spanning the time from cycle $\text{E}459 \pm 1$ to the start of $\text{E}457 \pm 1$ of Laskar et al., 2011, and Laskar, 2020), where the final parts of $\text{E}458$ and the start of $\text{E}457$ are interrupted by the onset of the Late Pliensbachian Event (Fig. 1). This longer record allows us to more robustly examine the influence of the long eccentricity cycle and the potential impact of a global carbon cycle perturbation on the palaeoclimate and depositional environment. We find that the long-eccentricity forcing continued to dictate the precise timing of major environmental changes in the Cardigan Bay Basin, including the initial step of the positive carbon isotope excursion.

2 Material

2.1 Palaeo-location and setting

Associated with the break-up of Pangaea, connections between oceans via epicontinental seaways were established during the Early Jurassic, such as the Hispanic Corridor, which connected the north-western Tethys and the eastern Panthalassa, and the Viking Corridor which linked the north-western Tethys Ocean to the Boreal Sea (Sellwood and Jenkyns, 1975; Smith, 1983; Bjerrum et al., 2001; Damborenea et al., 2013). The linking passage of the NW Tethys Ocean and the Boreal Sea (south of the Viking Corridor) is the palaeo-geographical location of the Llanbedr (Mochras Farm) borehole, Cardigan Bay Basin, NW Wales, UK (Fig. 2) – referred to hereafter as Mochras. Due to the location of the Mochras succession during the late Pliensbachian, it was subject to both polar and equatorial influences allowing the study of variations in the circulation in the N–S Laurasian Seaway (including the Viking Corridor) prior to and across the LPE. Mochras was located at a mid-palaeo-latitude of $\sim 35^\circ\text{N}$ (see Torsvik and Cocks, 2017).

The depositional environment of Mochras is likely characterized by a rift setting, which is reflected by the relatively

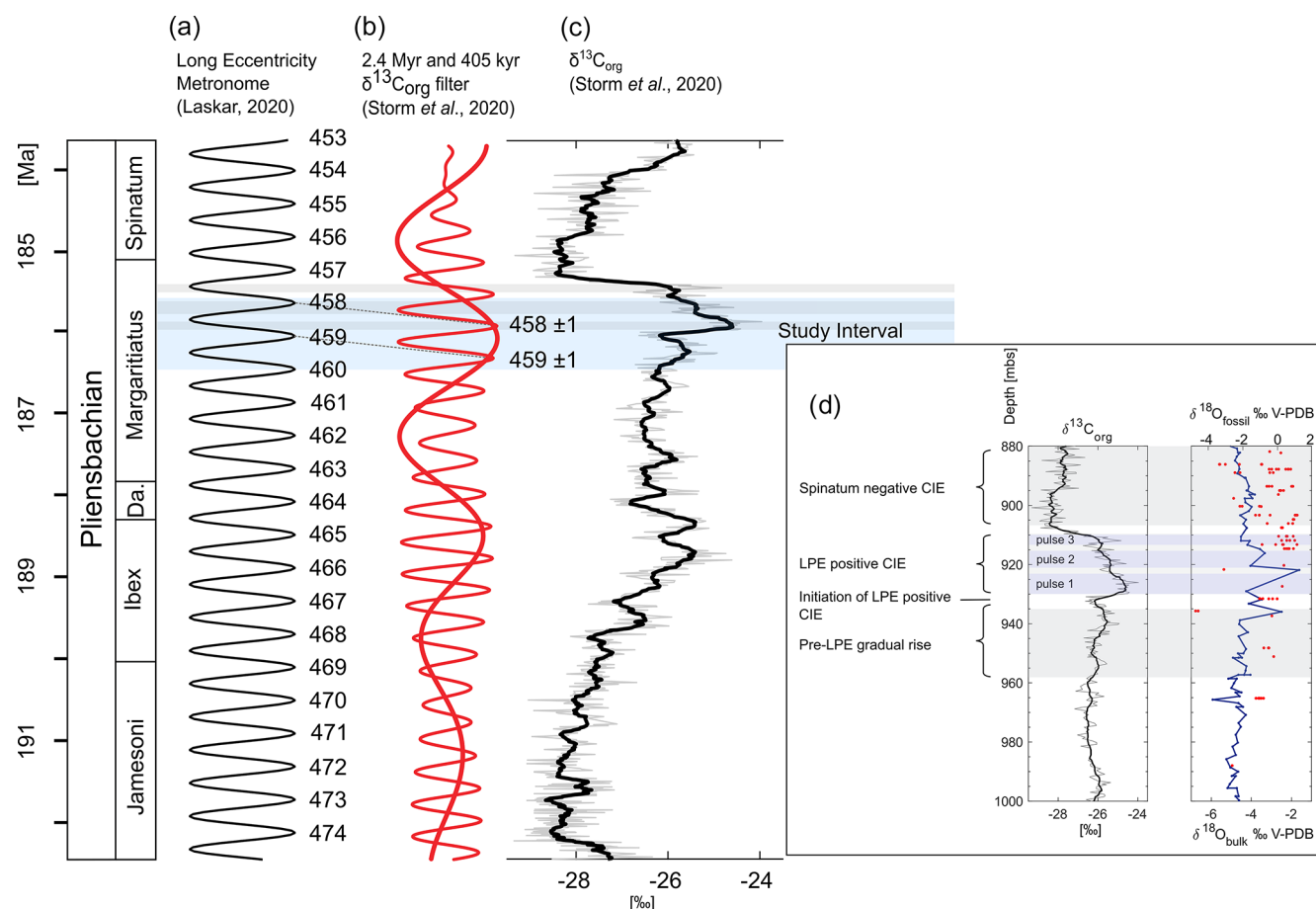


Figure 1. Stratigraphic framework of the Mochras borehole. **(a)** The 405 kyr metronome (Laskar, 2020), which shows that this study spans $E459 \pm 1$ and $E458 \pm 1$. **(b)** The 2.4 Myr and 405 kyr filters derived from the $\delta^{13}\text{C}_{\text{org}}$ record from Storm et al. (2020). A slight offset in pacing is observed in the 405 kyr metronome based on an assumed fixed 405 kyr cycle length **(a)**, versus filtering of the 405 kyr signal from the orbital solution **(b)**. **(c)** $\delta^{13}\text{C}_{\text{org}}$ curve from the Mochras borehole (Storm et al., 2020), showing the $\sim 1.8\text{‰}$ + CIE that marks the LPE. High-resolution data are visualized in light grey and a 10-step moving average in black. The blue bar marks interval in the Mochras borehole considered in this study. The three grey shaded bars represent the three pulses in the positive CIE of the LPE. **(d)** Close-up of the $\delta^{13}\text{C}_{\text{org}}$ (Storm et al., 2020) and $\delta^{18}\text{O}_{\text{bulk}}$ and $\delta^{18}\text{O}_{\text{fossil}}$ (Ullmann et al., 2022) from the late Pliensbachian of the Mochras core. A pre-LPE gradual rise is recorded in the $\delta^{13}\text{C}_{\text{org}}$, followed by the initiation of the LPE positive CIE, which consists of three pulses. After the LPE positive CIE, $\delta^{13}\text{C}_{\text{org}}$ values drop, recorded starting at ~ 910 m. b.s., and the Spinatum negative CIE is recorded. The $\delta^{18}\text{O}_{\text{bulk}}$ of the Mochras core (blue) is diagenetically altered and unlikely to preserve a palaeoclimatic imprint (Ullmann et al., 2022). Also, shown are $\delta^{18}\text{O}_{\text{fossil}}$ values (red).

open and deep marine facies and the evidence for below-storm wave-base and contourite deposition (Pieńkowski et al., 2021) but always with a strong terrestrial influence (van de Schootbrugge et al., 2005; Riding et al., 2013) from the nearby landmasses (Dobson and Whittington, 1987). The Cardigan Bay Basin fill was downthrown against the early Paleozoic Welsh Massif by a major normal fault system, probably comprising the Bala, Mochras, and Tonfanau faults at the eastern and south-eastern margins of the basin in late Paleozoic–early Mesozoic time (Woodland, 1971; Tappin et al., 1994). The main source of detrital material is understood to be the Caledonian Welsh Massif, followed by the Irish and Scottish landmasses (Deconinck et al., 2019). Other massifs that could have influenced the provenance are the London–

Brabant Massif to the south-east and Cornubia to the south (van de Schootbrugge et al., 2005), depending on the marine circulation and sediment transport at the time.

2.2 Core location and material

The Llanbedr (Mochras Farm) borehole was drilled onshore in the Cardigan Bay Basin ($52^{\circ}48'32''$ N, $4^{\circ}08'44''$ W) in 1967–1969, North Wales (Woodland, 1971; Hesselbo et al., 2013). The borehole recovered a 1300 m thick Early Jurassic sequence (601.83–1906.78 m. b.s. – metres below surface), yielding the most complete and extended Early Jurassic succession in the UK, being double the thickness of same-age strata in other UK cores and outcrops (Hesselbo et al., 2013;

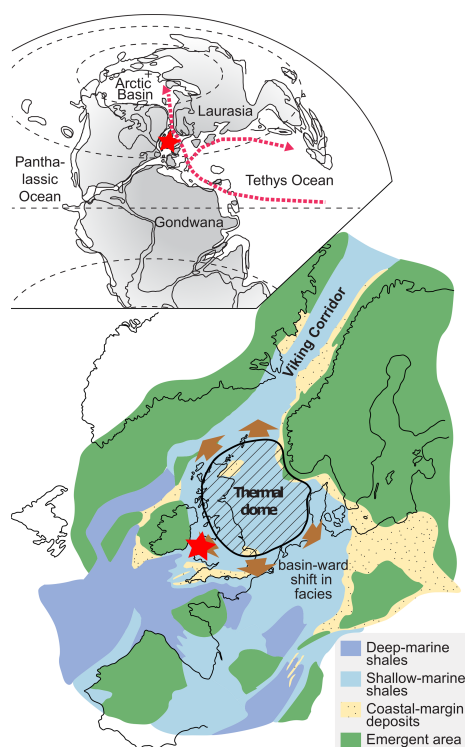


Figure 2. Palaeo-location of the Mochras borehole in the context of potential North Sea doming. Figure reprinted and adapted from Korte et al. (2015), which is open access (<https://creativecommons.org/licenses/by/4.0/>, last access: 1 November 2022). The Mochras borehole was located at a palaeo-latitude of $\sim 35^\circ$ N in the Cardigan Bay Basin (Torsvik and Cocks, 2017). Circulation in the Tethys Ocean and between it and the Boreal region influenced the depositional environment of the Mochras core (Pieńkowski et al., 2021). Late Pliensbachian sea level fall potentially resulted in the occlusion of the Viking Corridor as the topography of the North Sea dome structure disrupted circulation in the seaward (Korte et al., 2015).

Ruhl et al., 2016). The Lower Jurassic is biostratigraphically complete at the zonal level (Ivimey-Cook, 1971; Copestake and Johnson, 2014), with the top truncated and unconformably overlain by Cenozoic strata (Woodland, 1971; Dobson and Whittington, 1987; Tappin et al., 1994; Hesselbo et al., 2013). The lithology is dominated by argillaceous sediments, with alternating muddy limestone, marl, and mudstone (Woodland, 1971; Sellwood and Jenkyns, 1975).

The Pliensbachian Stage in the Mochras borehole occurs between ~ 1250 and ~ 865 m. b.s., with the Margaritatus Zone between ~ 1013 and 909 m. b.s. (Kevin N. Page in Copestake and Johnson, 2014). The Pliensbachian interval comprises alternations of mudstone (with moderate TOC) and organic-poor limestones, with a pronounced cyclicity at a $\sim 1 \pm 0.5$ m wavelength (Ruhl et al., 2016). The upper Pliensbachian contains intervals that are silty and locally sandy, whilst levels of relative organic enrichment also occur through the Pliensbachian (Ruhl et al., 2016). Overall, the

upper Pliensbachian is relatively rich in carbonate (Ruhl et al., 2016; Ullmann et al., 2022).

3 Methods

For this study, samples were taken at a ~ 30 cm resolution from slabbed core from 934–918 m. b.s. for X-ray diffraction (XRD) and mass spectrometry, as well as palynofacies and microcharcoal analysis. X-ray fluorescence (XRF) analyses were made at a 1 cm resolution from 934–918 m. b.s. (complete dataset deposited as Damaschke et al., 2021). These new samples complement samples and data at a 10 cm resolution from 951–934 m. b.s. published in Hollaar et al. (2021).

3.1 TOC, CaCO_3 , and bulk organic carbon isotope mass spectrometry

TOC and $\delta^{13}\text{C}_{\text{org}}$ were measured to track the changes in the total organic carbon fraction and the bulk organic carbon isotope ratios in relation to the other palaeoenvironmental proxy data.

Powdered bulk rock samples (~ 2 g) were decarbonated in 50 mL of 3.3 % HCl. After this, the samples were transferred to a hot bath of 79°C for 1 h to remove siderite and dolomite. Subsequently, the samples were centrifuged and the liquid decanted. The samples were rinsed repeatedly with distilled water to reach neutral pH. After this, the samples were oven-dried at 40°C , re-powdered, and weighed into tin capsules for mass spectrometry using the Sercon Integra 2 stable isotope analyser at the University of Exeter Environment and Sustainability Institute (ESI), stable isotope facility on the Penryn Campus, Cornwall. Samples were run alongside in-house reference material (bovine liver: $\delta^{13}\text{C} -28.61$; alanine: $\delta^{13}\text{C} -19.62$) which was used to correct for instrument drift and to determine the $\delta^{13}\text{C}$ values of the samples. The $\delta^{13}\text{C}_{\text{org}}$ values are reported relative to V-PDB (Vienna Peedee Belemnite) following a within-run laboratory standard calibration. Total organic carbon was determined using the CO_2 beam area relative to the bovine liver standard (% C 47.24). Replicate analysis of the in-house standards gave a precision of $\pm < 0.1\text{‰}$ (2 SD).

The carbonate content was measured by the dry weight sample loss before and after decarbonation. The carbon percentage content derived from the mass spectrometer was corrected for carbonate loss to derive TOC.

3.2 XRD to determine clay mineralogy

Clay mineral analysis was performed to gain insight into the relative importance of physical erosion versus chemical weathering and related changes in the hydrological cycle.

About 2–3 g of gently powdered bulk rock was decarbonated with a 0.2 M HCl solution. The clay sized fraction ($< 2\ \mu\text{m}$) was extracted with a syringe after decantation of

the suspension after 95 min following Stokes' law. The extracted fraction was centrifuged and oriented on glass slides for XRD analysis using a Bruker D4 Endeavour diffractometer (Bruker, Billerica, MA, USA) with Cu $K\alpha$ radiations, LynxEye detector, and Ni filter under 40 kV voltage and 25 mA intensity (Biogéosciences Laboratory, Université Bourgogne/Franche-Comté, Dijon). Following Moore and Reynolds (1997), the clay phases were discriminated in three runs per sample: (1) air-drying at room temperature; (2) ethylene-glycol solvation for 24 h under vacuum; (3) heating at 490 °C for 2 h.

Identification of the clay minerals was based on their main diffraction peaks and on comparison of the three diffractograms obtained. The proportion of each clay mineral on glycolated diffractograms was measured using the MACD-IFF 4.2.5. software (Petschick, 2000). Identification of the clay minerals follows the methods in Deconinck et al. (2019) and Moore and Reynolds (1997).

3.3 Palynofacies and microcharcoal

Palynofacies were examined to explore shifts in the terrestrial versus marine origins of the particulate organic matter. Each ~ 20 g bulk rock sample was split into 0.5 cm³ fragments, minimizing breakage of charcoal and other particles, to optimize the surface area for the extraction of organic matter using a palynological acid maceration technique. The samples were first treated with cold hydrochloric acid (10 % and 37 % HCl) to remove carbonates. Following this, hydrofluoric acid (40 % HF) was added to the samples to remove silicates. Carbonate precipitation was prevented, by adding cold concentrated HCl (37 %) after 48 h. The samples were neutralized via multiple dilution–settling–decanting cycles using DI (distilled) water, after which five droplets of the mixed residue were taken for the analysis of palynofacies prior to sieving. The remaining residue was sieved through a 125 and 10 μ m mesh to extract the microcharcoal fraction.

A known quantity (11 μ L) out of a known volume of liquid containing the 10–125 μ m sieved residue was mounted onto a palynological slide using glycerine jelly. This fraction, containing the microscopic charcoal, was analysed and the charcoal particles counted using an Olympus (BX53) transmitted light microscope (40 \times 10 magnification). For each palynological slide, four transects (two transects in the middle and one on the left and right side of the coverslip) were followed and the number of charcoal particles determined. Charcoal particles were identified with the following criteria: opaque and black, often elongated lath-like shape with sharp edges, original anatomy preserved, and a brittle appearance with a lustrous shine (Scott, 2010). These data were then scaled up to the known quantity of the sample according to the method of Belcher et al. (2005).

Palynofacies were grouped broadly according to Obokken et al. (2005): sporomorphs, fungal remains, freshwater algae, marine palynomorphs, structured phytoclasts,

unstructured phytoclasts, black debris, amorphous organic matter (AOM), and charcoal (further described in Hollaar et al., 2021). The palynofacies were quantified on a palynological slide using the optical light microscope (40 \times 10 magnification) and counting a minimum of 300 particles per slide. Because the samples are AOM-dominated, counting was continued until a minimum of 100 non-AOM particles were observed. We used the percentage of terrestrial phytoclasts, which includes sporomorphs, and structured and unstructured phytoclasts to examine changes in terrestrial organic particle content.

3.4 XRF to determine detrital elements

Detrital elemental ratios were examined to analyse changes in relative terrestrial influx and the type of material transported from the land to the marine realm. The slabbed archive halves of the Mochras borehole were scanned via automated XRF at a 1 cm resolution for the interval 951–918 m. b.s., with the The Itrax multi-core (MC) at the British Geological Survey Core Scanning Facility (CSF), Keyworth, UK (Damaschke et al., 2021). The measurement window was 10 s and long-term drift in the measurement values was counteracted by regular internal calibration with a glass reference (NIST-610). Duplicate measurements were taken every 5 m for a 50 cm interval to additionally verify the measured results.

3.5 Statistical analysis

Principal component analysis (PCA) was performed to examine a potential change in the proxy data before and after the positive CIE. This was executed in the software PAST on the normalized dataset including microcharcoal, TOC, CaCO₃, $\delta^{13}\text{C}_{\text{org}}$, S/I, K/I, primary clay mineralogy, Si/Al, and Zr/Rb. The samples before the positive CIE (951.0–930. m. b.s.) and the samples after the positive CIE (930.3–918.0 m. b.s.) are grouped to examine a potential difference in the sedimentary composition before and after the positive CIE. A Pearson's correlation was executed in MATLAB R2017b. The p value tests the hypothesis of no correlation against the alternative hypothesis of a positive or negative correlation (significance level at $p \leq 0.05$).

4 Results

4.1 TOC, CaCO₃, and bulk organic carbon isotope ratio mass spectrometry

Alternating TOC-enhanced and Ca-rich lithological couplets occur on a metre scale through the studied interval, with TOC and CaCO₃ having a strong negative correlation ($r = -0.64$, $p = 0.001$). TOC content fluctuates in the range of 0.17–1.72 wt % (mean 0.8 wt %), and the highest fluctuations in TOC content are found from 939–930 m. b.s. The CaCO₃ content fluctuates in opposition to TOC and varies between

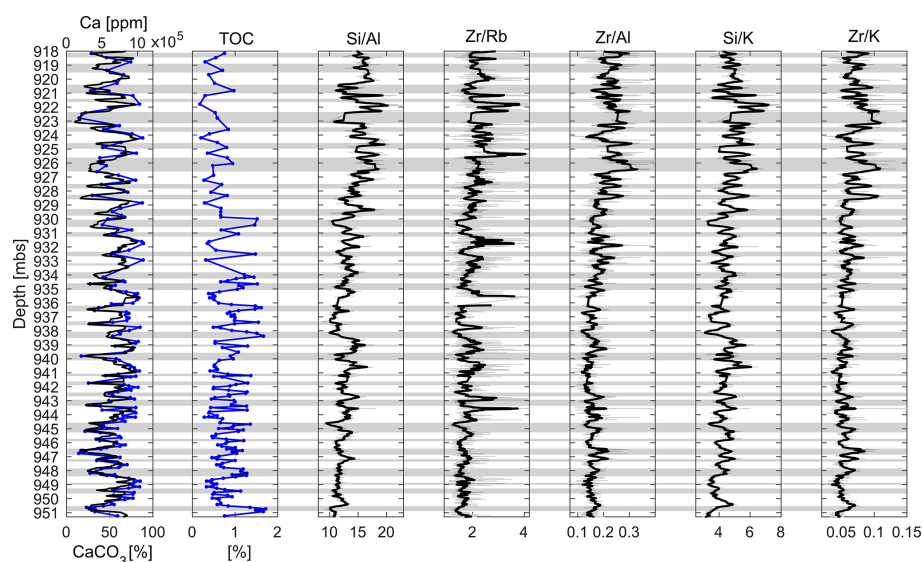


Figure 3. Detrital ratios over the Ca-rich and TOC-enhanced lithological couplets for the studied interval. Overview of Ca (black, derived from Ruhl et al., 2016), CaCO_3 (blue), and TOC content of the studied interval 951–918 m. b.s. The grey shading represents the TOC-enhanced beds and the unshaded bands mark the Ca-rich (limestone) beds. The detrital ratios reflect the silt to fine sand fraction (Si, Zr) versus the clay fraction (Rb, Al, K). Two increasing-upward cycles are observed in the Si/Al and Zr/Rb ratios. The pattern observed in all detrital ratios (except Ti/Al) is similar and likely reflects overall upward coarsening.

14 % and 89 %. The studied interval is generally high in CaCO_3 (mean 58 %) (Fig. 3). The $\delta^{13}\text{C}_{\text{org}}$ displays a minor ($\sim 0.5\text{‰}$) shift towards more positive values at ~ 944 m. b.s. (as reported in Storm et al., 2020; Hollaar et al., 2021). At ~ 930 m. b.s. an abrupt shift of $\sim 1.8\text{‰}$ (Figs. 1 and 4; Storm et al., 2020) indicates the onset of the Late Pliensbachian Event (LPE) in the Mochras core. In agreement with this, the results of the present study show a shift from $\sim -27\text{‰}$ to $\sim -25.15\text{‰}$ between 930.8 and 930.4 m. b.s. (Fig. 4). The $\delta^{13}\text{C}_{\text{org}}$ data presented here have been divided into three phases: the pre-LPE gradual rise, followed by the positive CIE, which is subdivided into pulses 1, 2, and 3 (Fig. 1). After the onset of the positive $\delta^{13}\text{C}_{\text{org}}$ excursion, the TOC content drops to the lowest values (from 0.85 % before and 0.6 % after the positive CIE on average), but the 1 m fluctuations continue (Figs. 3 and 4). No overall change in the CaCO_3 content is observed through the positive carbon isotope excursion (Fig. 3).

4.2 Clay minerals

XRD analysis shows that the main clay types found in this interval are illite, random illite–smectite mixed layers (I-S R0) (hereafter referred to as smectite), and kaolinite. Illite and kaolinite co-fluctuate in the interval studied here and are directly out of phase with smectite abundance. Chlorite and I-S R1 are present in minor proportions but reach sporadically higher relative abundance ($> 10\%$) from ~ 932 m. b.s. upwards, with sustained $> 10\%$ abundance at ~ 925 – 918 m. b.s. (Figs. 4 and S1 in the Supplement). The

relative abundances of smectite and illite and of kaolinite and illite are expressed by the ratio S/I and K/I, respectively. These ratios were calculated according to the intensity of the main diffraction peak of each mineral.

4.3 Organic matter

The type of particulate organic matter, and more specifically the abundance in the marine versus terrestrial origin of the particles, fluctuates on a metre scale from 18 %–42 % (Figs. 4 and S2). Palynofacies indicate that the type of organic matter does not change in relation to the metre-scale lithological facies cycles (no correlation between percentage terrestrial phytoclasts and TOC or CaCO_3). No large and abrupt changes are recorded in the terrestrial/marine proportions, but the proportion of terrestrial phytoclasts has four high phases: between 944.6 and 942.0 m. b.s., 937.5 and 934.9 m. b.s., 930.4 and 925.4 m. b.s., and 920.3 and 918.0 m. b.s. (Fig. S2). The first and second high phase falls within the $+0.5\text{‰}$ positive swing in the $\delta^{13}\text{C}_{\text{org}}$, whilst the latter two high phases correspond to pulse 1 and pulse 2 in the positive CIE. Amorphous organic matter (AOM) is very abundant, followed by unstructured phytoclasts, with lower proportions of structured phytoclasts and charcoal (Fig. S3). Charcoal particles make up a relatively large proportion of the terrestrial particulate organic matter ($\sim 10\%$ on average) and $\sim 3.5\%$ on average of the total particulate organic matter fraction (Fig. S3). Only sparse marine and terrestrial palynomorphs were observed (Fig. S3).

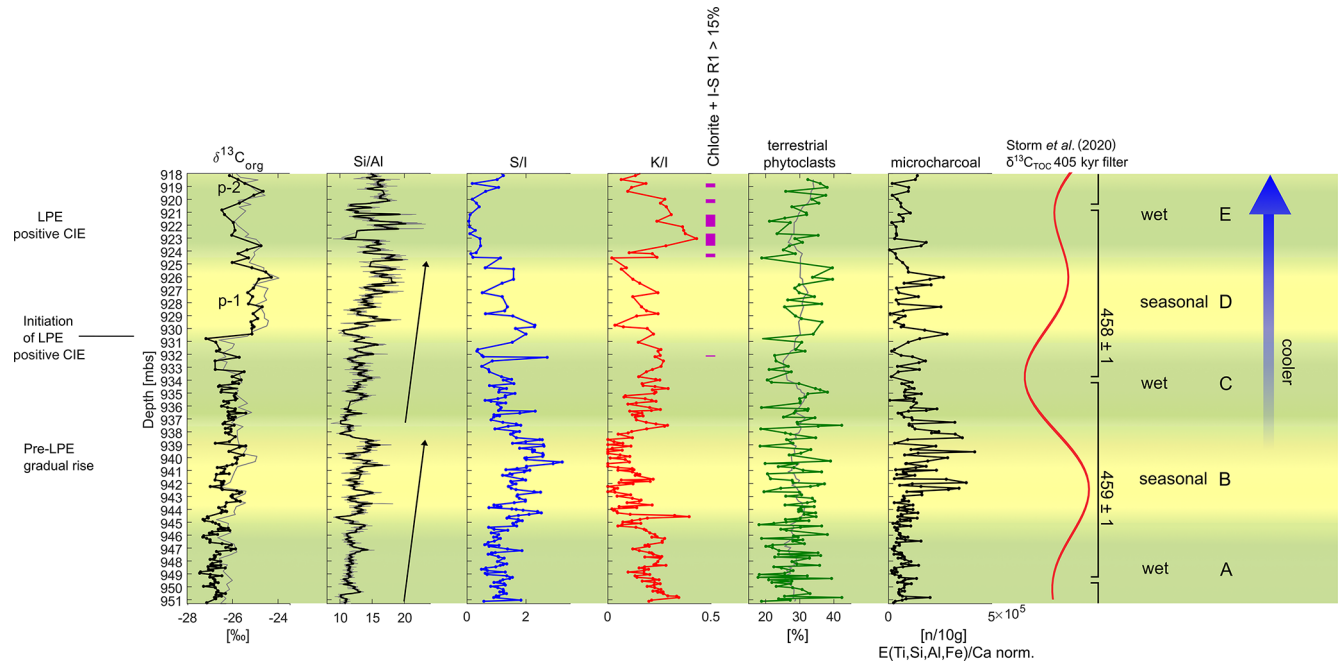


Figure 4. Synthesis diagram showing the climatic swings observed in tandem with the long eccentricity cycle. The studied interval (upper Pliensbachian Margaritatus Zone) comprises part of the pre-LPE gradual rise, the initiation of the LPE positive CIE, and pulses 1 and 2 ($\delta^{13}\text{C}_{\text{org}}$ data in black from this study and in light grey from Storm et al., 2020). Five climatic phases (A–E) are interpreted from Si/Al, smectite / illite, kaolinite / illite, chlorite, and I-S R1 abundance, and the microcharcoal abundance. In tandem with the 405 kyr cycle (Storm et al., 2020), the climatic state of a year-round wet climate, low fire activity, and fine-grained sediments across multiple precession cycles (phases A and C) alternates with a climatic state that includes repeated precessionally driven states that are semi-arid, with high fire activity and coarser sediments (phases B and D). The top of the record (phase E) indicates increased physical erosion (chlorite + I-S R1, kaolinite) relative to chemical weathering. In the terrestrial phytoclast column, the grey line shows the 10-step moving average.

To assess the character of the observed fluctuations in microcharcoal abundance, whether changes in microcharcoal can be related to enhanced runoff from the land and/or organic preservation, or whether the microcharcoal signifies changes in fire activity on land, the charcoal record was corrected for detrital influx. We adjust the charcoal particle abundances using the XRF elemental record, normalizing to the total terrigenous influx following Daniau et al. (2013) and Hollaar et al. (2021). The stratigraphic trends in the normalized microcharcoal for E_{ter}/Ca , Si/Al, Ti/Al, and Fe/Al remain the same (Fig. S4). The absolute number of microcharcoal particles decreases, with 1.06×10^5 per 10 g of raw mean charcoal particles and E_{ter}/Ca normalized mean 9.7×10^4 number of charcoal particles (hereafter denoted n) per 10 g, Ti/Al normalized 6.4×10^4 n per 10 g, Si/Al normalized 7.7×10^4 n per 10 g, and Fe/Al normalized 9.8×10^4 mean number of microcharcoal particles per 10 g (Fig. S4). The number of microcharcoal particles per 10 g of processed rock decreases when correcting for terrestrial runoff changes, hinting that perhaps part of the “background” microcharcoal is related to terrestrial influx; the normalization also shows that the observed patterns in microcharcoal abundances are not influenced by changes in terrestrial runoff and taphonomy. Hence, the highs and lows in the microcharcoal record

can be interpreted as representing changes in the fire regime on land. The microcharcoal abundance fluctuates strongly in the record presented here; however, no clear difference in microcharcoal content has been observed before and after the onset of the positive CIE.

4.4 Detrital elemental ratios (XRF)

Strong similarities are observed between the fluctuating ratios of Si/Al, Si/K, Zr/Rb, Zr/Al, and Zr/K (Fig. 3). The elements Al, Rb, and K sit principally in the clay fraction (e.g. Calvert and Pederson, 2007), whereas Si and Zr are often found in greater abundance in the coarser fraction related to silt and sand grade quartz and heavy minerals (Calvert and Pederson, 2007). The ratios all show clear metre-scale fluctuations, and these are superimposed on two increasing-upward trends observed in both Si/Al and Zr/Rb, followed by a drop and rise to peak values in the latest part of phase D and phase E above the onset of the positive CIE (Figs. 3 and 4). A parallel trend is observed between the clay ratios (XRD) and elemental ratios Si/Al and Zr/Rb (Fig. 3). Phases of high S/I correspond to the peaks in the two coarsening-upward sequences, whereas phases of high K/I correspond to the low phases in the two coarsening-upward sequences.

After the positive CIE onset (in phase E) this relationship turns around, and an enrichment in the kaolinite / illite ratio corresponds to the elemental ratios, where highest kaolinite relative abundance is observed in parallel with elemental ratios suggesting a maximum coarse fraction.

4.5 PCA

The proxy datasets ($\delta^{13}\text{C}_{\text{org}}$, TOC, percentage of terrestrial phytoclasts, microcharcoal, smectite/illite, kaolinite/illite, abundance of chlorite and I-S R1, Si/Al, Zr/Rb, Zr/Al) were normalized between 0–1 and run for PCA in PAST. Sixty-four percent of the variance is explained by the first three axes (PCA-1 27.7 %, PCA-2 19.7 %, PCA-3 15.3 %) inside the 95 % confidence interval.

PC-1 (PC – principal component) mainly explains the anti-correlation of TOC and CaCO_3 . PC-2 shows the anti-correlation of K/I and S/I. Positive loadings were observed for S/I, microcharcoal, macrocharcoal, and CaCO_3 . For PC-2, negative loadings were observed for K/I, and abundance of chlorite and I-S R1. PC-3 shows strong positive loadings (> 0.3) for $\delta^{13}\text{C}_{\text{org}}$, Si/Al, and Zr/Al.

Plotting PC-1 (y axis) over PC-3 (x axis) shows that after the onset of the positive CIE the samples are grouped to the top of the y axis (more associated with S/I compared to K/I) and to the right of the x axis (more associated with primary minerals, phytoclasts, and higher Si/Al, Zr/Rb, and Zr/Al) (Fig. 5).

5 Discussion

Figure 1 provides the context for the LPE “cooling event” at Mochras set within the background record. Shifts in bulk $\delta^{18}\text{O}_{\text{carb}}$ are coeval to the $\delta^{13}\text{C}_{\text{org}}$ change to heavier isotopic values (~ 930 m. b.s.) and reach a maximum in the Margaritatus Zone ($> 1\%$) (Ullmann et al., 2022). The bulk oxygen-isotope excursions of Mochras are affected by diagenesis and are deemed unlikely to reflect environmental conditions (Ullmann et al., 2022). However, oxygen-isotope data from marine benthic and nekto-benthic molluscs and brachiopods show heavier values during the late Margaritatus Zone concurrent with a positive shift in $\delta^{13}\text{C}_{\text{org}}$, indicating cooling during the LPE in the nearby Cleveland Basin (Robin Hood’s Bay and Staithes) (Korte and Hesselbo, 2011), and this trend is also observed in several European sections (e.g. Korte et al., 2015). The duration of the positive CIE has been estimated as ~ 0.4 – 0.6 Myr in the Cardigan Bay Basin (Ruhl et al., 2016; Storm et al., 2020; Pieńkowski et al., 2021).

5.1 Background sedimentological and environmental variations

The Mochras succession shows metre-scale, alternating TOC-enhanced and Ca-rich lithological couplets (mudstone/limestone; Fig. 3). Previous assessments of the

palaeoenvironmental signature of these TOC-enhanced and Ca-rich couplets indicate strongly that the different depositional modes are driven by orbital precession (Ruhl et al., 2016; Hinnov et al., 2018; Storm et al., 2020; Hollaar et al., 2021; Pieńkowski et al., 2021). Precession-driven changes in monsoonal strength have been suggested to influence the deposition and preservation of TOC and carbonate in the Cardigan Bay Basin (Ruhl et al., 2016), although the impact may have been expressed, at least partially, by changes in the strength of bottom currents in the seaway as a whole (Pieńkowski et al., 2021).

The preservation of primary carbonate is poor in the Mochras borehole, making it complex to determine in detail the relative importance of carbonate producers for the bulk carbonate content (Ullmann et al., 2022). However, Early Jurassic, pelagic settings in the Tethys region often received abiotic fine-grained carbonate from shallow marine carbonate platforms (Weedon, 1986; Cobianchi and Picotti, 2021; Krencker et al., 2020) and partly via carbonate producing organisms (such as coccolithophores in zooplankton pellets) (Weedon, 1986; van de Schootbrugge et al., 2005, e.g. Weedon et al., 2019; Slater et al., 2022). Coccolithophores are often poorly preserved and recrystallized (Weedon, 1986; Weedon et al., 2019; Slater et al., 2022). The organic matter found in the studied section of the Mochras borehole varies between 18 % and 42 % of terrestrial phytoclasts (Fig. 4). Phytoclasts are common, but palynomorphs are relatively sparse and poorly preserved. Marine amorphous organic matter is the main constituent in the present study of particulate organic matter in unsieved macerated samples in the interval studied here (951–918 m. b.s.). An examination of variations in the terrestrial/marine proportions of organic matter shows no correspondence between the type of organic matter and the TOC-enhanced or Ca-rich lithological alternations. However, previous research has indicated that the percentage of terrestrial phytoclasts shows precession forcing independent of the lithological couplets (so out of phase with precession-scale changes in Ca-TOC content) between 951–934 m. b.s. in the Mochras core (Hollaar et al., 2021). Such orbital forcing of the terrestrial vs. marine proportions of organic matter was also found in Early Jurassic sediments of Dorset and was similarly independent of the lithological facies (Waterhouse, 1999). Terrestrial phytoclast content shows a weak expression of long-eccentricity-driven variations in the section studied (Fig. 4).

Fossil charcoal makes up a substantial proportion of the organic fractions (11 % of the terrestrial fraction) and has previously been shown to vary considerably over long eccentricity cycle 459 ± 1 peaking in abundance during the phase of maximum eccentricity (Hollaar et al., 2021). Micro-charcoal also appears to be most abundant during the maximum phase of the subsequent long eccentricity cycle 458 ± 1 (Fig. 4). Additionally, K/I and S/I clay mineral ratios appear to alternate in response to long-eccentricity drivers (Fig. 4) up to 931 m. b.s., where the clay mineral signature changes. De-

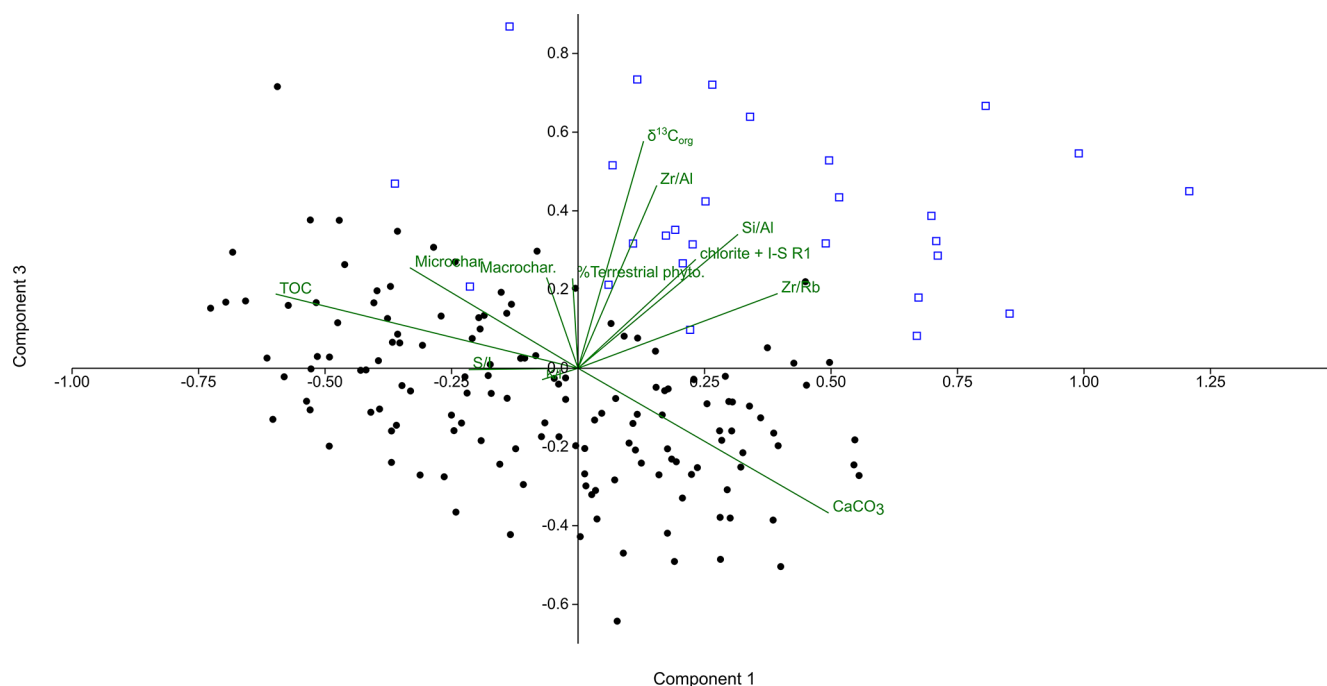


Figure 5. PCA shows a distinctly different depositional signature before and after the onset of the LPE positive CIE in the Mochras core. PCA plot of PC-1 and PC-3: all samples before the onset of the LPE positive CIE are marked by closed black circles and the samples after the onset of the LPE positive CIE are marked by open blue squares.

trital clays form in soil weathering profiles and/or physical weathering of bedrock. Chemical weathering is enhanced in a high-humidity environment with relatively high temperatures and rainfall, when clays are formed in the first stages of soil development. In the modern day, kaolinite is primarily formed in tropical soils, under year-round rainfall and high temperatures (Thiry, 2000). Smectite also occurs in the tropics but is more common in the subtropical to Mediterranean regions, where humidity is still high but periods of drought also occur (Thiry, 2000). Hence, smectite forms predominantly in soil profiles under a warm and seasonally dry climate (Chamley, 1989; Raucsik and Varga, 2008) and kaolinite in a year-round humid climate (Chamley, 1989; Ruffell et al., 2002). Similarly, alternating intervals of kaolinite and smectite dominance were observed for the late Sinemurian (Munier et al., 2021) and the Pliensbachian of Mochras (Deconinck et al., 2019).

The predominantly detrital character of these clay minerals has been confirmed by TEM (transmission electron microscopy) scanning of Pliensbachian smectite minerals, which revealed the fleecy morphology and lack of overgrowth (Deconinck et al., 2019). Therefore, the alternations of smectite and kaolinite are interpreted as reflecting palaeoclimatic signatures of a changing hydrological cycle, with a year-round wet climate evidenced by high K/I ratios and a more monsoon-like climate with seasonal rainfall with high S/I (Deconinck et al., 2019; Hollaar et al., 2021; Munier et al., 2021) (see Figs. 3 and 6). The intervals with a signal

for weaker seasons appear to correspond to phases of low eccentricity in the 405 kyr cycle and signals of greater seasonality with periods of high more pronounced eccentricity (Fig. 4) in the 405 kyr cycle. Between 951 and 930 m. b.s. high K/I occurs during phases of low long eccentricity suggesting an enhanced hydrological cycle (Hollaar et al., 2021) with more intense weathering and enhanced fine-grained terrestrial runoff to the marine record (Deconinck et al., 2019). In contrast, phases of maximum long eccentricity appear to be smectite-rich, indicating seasonal rainfall, enhanced fire (Hollaar et al., 2021) and thus periods of droughts, and lower terrestrial runoff and subsequent lower dilution (Deconinck et al., 2019).

Detrital elemental ratios increase accordingly during the smectite-rich phases and are lower during kaolinite-rich phases between 951 and 930 m. b.s. Detrital elemental ratios can be used to explore changes in sediment composition (e.g. Thibault et al., 2018; Hesselbo et al., 2020b), and the similarity of the long-term trend in Zr/Rb and Si/Al (Fig. 3) indicates that these elemental ratios reflect grain size. The clay fraction (hosting Al, and Rb; Chen et al., 1999), diminishes upwards, whereas the coarser silt to sand fraction (associated with Si: Hesselbo et al., 2020b; associated with Zr: Chen et al., 2006), increases upward (Figs. 3 and 4). The grain size changes inferred here reflect two overall coarsening-upward sequences (Figs. 3 and 4). These sequences may reflect changes in clastic transport due to changes in the proximity to the shore/siliciclastic source,

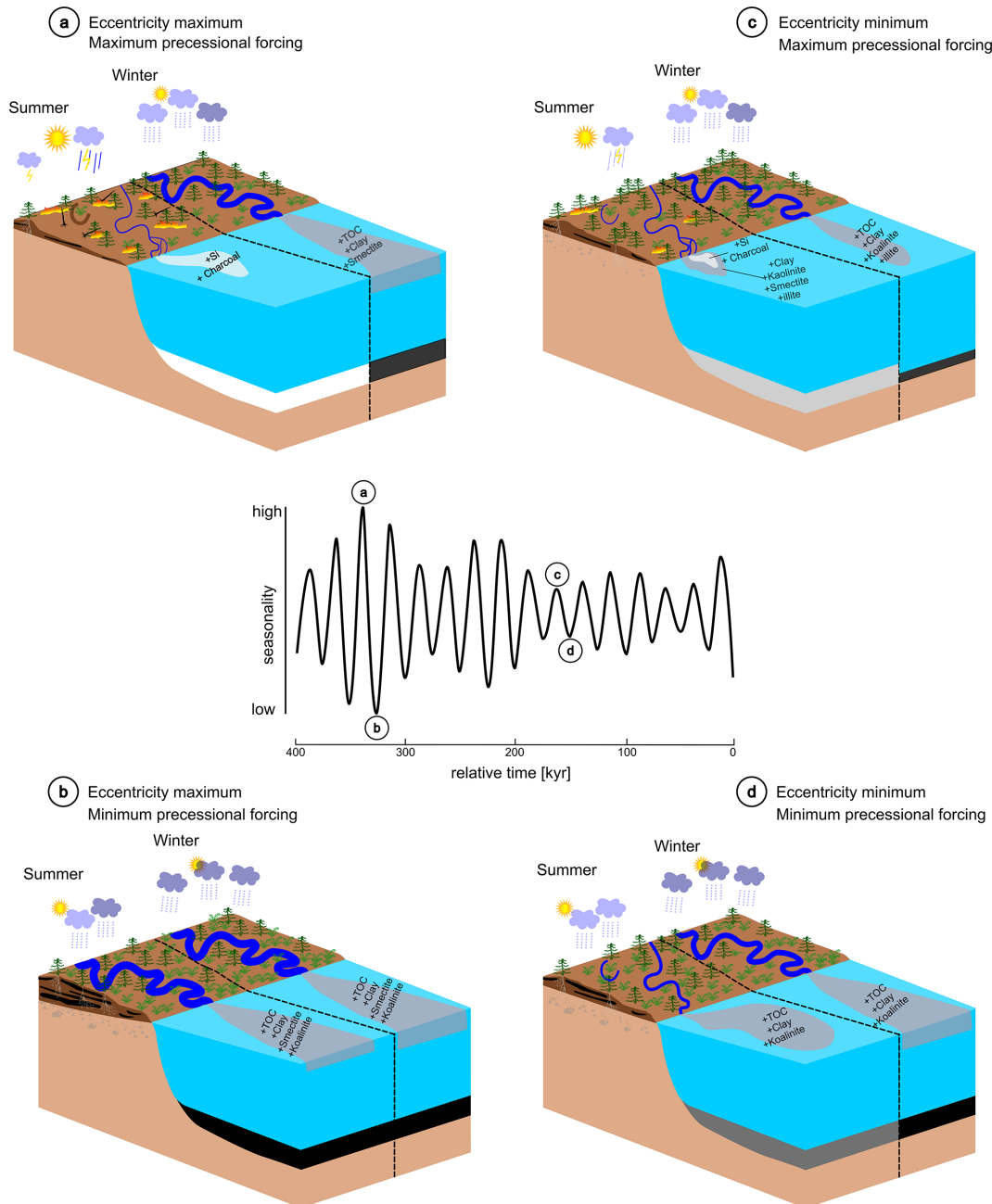


Figure 6. Scheme of four environmental scenarios under the influence of eccentricity on a precessional timescale. **(a)** The most extreme seasonal contrast in the Northern Hemisphere occurs during maximum precessional forcing (i.e. low-precession index) and maximum amplitude modulation by eccentricity. The seasonal contrast leads to a wet season that allows biomass to build up, high terrestrial runoff, and relatively enhanced organic burial in marine settings. During the dry season, fuel moisture levels are lower and fires are rapidly ignited and spread. Intensified monsoonal rains may lead to enhanced coarse-grained terrestrial runoff. Overall, less terrestrial runoff during this dry season results in less dilution of carbonate production and/or less primary productivity of organic plankton. **(b)** Minimum precessional forcing and maximum amplitude modulation of eccentricity leads to the least seasonal contrast. Chemical weathering on land is more intense during this year-round humid climate. And although biomass is abundant, fire is suppressed due to the high moisture status. Both seasons are humid and have considerable terrestrial runoff, resulting in marine organic burial. **(c)** Moderate seasonality occurs during maximum precessional forcing and minimum amplitude modulation of the eccentricity cycle. During the wet season biomass grows, and during the dry season fires can occur due to drier fuel conditions. However, due to a lesser seasonal contrast, the dry conditions are less pronounced and fire is not widespread. Runoff includes coarse- and fine-grained sediments and charcoal during the dry season. **(d)** The seasonal contrast is low during minimum precessional forcing and the minimum amplitude modulation of the eccentricity cycle. Both seasons were humid and experienced runoff of fine-grained sediments and organic burial in marine settings. Moderately thick soil profiles could develop under this humid climate (figure developed from Martinez and Dera, 2015).

changes in runoff due to a changing hydrological cycle, changes in the intensity of weathering of the bedrock, or accelerated bottom currents with a greater carrying capacity for coarser sediments.

5.2 Depositional and environmental changes before and after the LPE positive CIE

5.2.1 Climate forcing of the hydrological cycle

The LPE positive CIE begins around 930 m. b.s. in the Mochras core and encompasses the remaining part of the studied section (Fig. 4). We contrasted all the pre-CIE sediment signatures with those of the positive CIE signatures using principal components analysis, which indicates distinctly different sedimentary composition and environmental signature before and after the onset of the positive CIE in Mochras (Fig. 5).

Before the positive CIE onset, the clay mineral assemblage shows alternating phases of smectite and kaolinite, indicating pedogenic weathering. The relative abundance of the detrital clay types observed in the studied interval has the potential to hold important palaeoclimatic information regarding the hydrological cycle and the relative proportion of chemical weathering and physical erosion. The hydrological cycle was forced by the 405 kyr eccentricity before the positive CIE, with alternating eccentricity maxima linked to enhanced seasonality (smectite) and eccentricity minima to an equitable wet climate (kaolinite) (Figs. 3 and 6). Higher-frequency cycles are not observed in the clay mineral ratios, with no precession or obliquity forcing detected in the high-resolution part of the study at 951–934 m. b.s. (Hollaar et al., 2021) and no expression of the 100 kyr cycle in the record presented here. The formation of developed kaolinite-rich, and to a lesser extent smectite-rich soil profiles, requires a steady landscape for many tens of thousands of years, although the ~ 1 Myr timescale of Thiry (2000) seems excessive in our case given the clear expression of clay mineral changes through long eccentricity cycles. Also, the transportation and deposition of continental clays will occur after soil formation and add further time between formation and final deposition (Chamley, 1989; Thiry, 2000). Thus, there is likely to be a lag of the climatic signal observed in the marine sediments (Chamley, 1989; Thiry, 2000). However, we note that high-frequency climatic swings have been recorded in the clay mineral record in some instances, such as in the Lower Cretaceous in SE Spain (Moiroud et al., 2012). The limestone–marl alternations there are enhanced in smectite versus kaolinite and illite, respectively, reflecting precession-scale swings from a semi-arid to a tropical humid climate (Moiroud et al., 2012). Precession and higher-frequency shifts in the clay record are likely caused by fluctuations in runoff conditions rather than the formation of soils with a different clay fraction.

Directly after the initial positive CIE shift from 930–924 m. b.s. (Phase 1 of Fig. 4) little seems to change, and the system evidently continued to respond as before to the long-eccentricity forcing, despite the predicted cooling (Korte and Hesselbo, 2011; Korte et al., 2015; Gómez et al., 2016). However, from around 924 m. b.s. up to the top of the studied section (Phase 2 of Fig. 4) the clay mineral assemblage displays a distinctly different composition, with kaolinite dominating especially the early part of phase 2 of the LPE (Fig. 4). At the same time there is an enhancement of the primary minerals illite and chlorite and I-S R1 (Figs. 4 and S1). Although an enhancement in detrital kaolinite indicates an acceleration of the hydrological cycle, detrital kaolinite is dual in origin and can also be derived from a reworking of the primary source material (Deconinck et al., 2019). If the climate is cooler, chemical weathering becomes less dominant and physical erosion of the bedrock becomes the main detrital source of clay minerals. In the Cardigan Bay Basin, the bedrock of the surrounding Variscan massifs (such as the Scottish, Welsh, and Irish massifs) were a likely source of these clays. In the Early Jurassic of the NW Tethys region, lower Paleozoic mudrocks bearing mica illite and chlorite were emergent (Merriman, 2006; Deconinck et al., 2019); hence the enhancement of illite and chlorite likely indicates physical erosion in the region surrounding the study site. Finally, authigenic clay particles could have been formed during burial diagenesis. At temperatures between 60–70 °C smectite illitization occurs and I-S R1 is formed; however, the high abundance of smectite in Mochras indicates limited burial diagenesis at that location (Deconinck et al., 2019). Weak to moderate thermal diagenesis is confirmed for the Pliensbachian of Mochras, with T_{\max} from pyrolysis analysis between 421 and 434 °C (van de Schootbrugge et al., 2005; Storm et al., 2020). Therefore, I-S R1 in Mochras is interpreted as being derived from chemical weathering of illite (Deconinck et al., 2019). The coeval increase in these primary clay minerals, I-S R1, and kaolinite indicates that during this period physical erosion dominated over soil chemical weathering (Deconinck et al., 2019; Munier et al., 2021). This is similar to what has been observed for the latest Pliensbachian in Mochras previously (Deconinck et al., 2019).

Erosion of weathering profiles transports clay minerals (including kaolinite and smectite) to the marine realm. In the ocean, the differential settling of kaolinite (near the shore) and smectite (more distal) could occur based on the morphology and size of clay particles (Thiry, 2000). However, a comparison of long-term inferred regional sea level changes from surrounding UK basins (Hesselbo, 2008) suggests that the relative proportions of smectite and kaolinite are not influenced by changes in relative sea level in the Pliensbachian of Mochras (Deconinck et al., 2019). On the assumption that the coarsening-upward sequences at Mochras are indicative of relative sea level change, it can also be argued that the proximity to the shore did not impact the proportions of smectite and kaolinite. Instead, we observe enhanced smectite dur-

ing “proximal” deposition and enhanced kaolinite at times of more “distal” deposition, the opposite of what might be expected (Fig. 4).

We suggest that the first phase of the LPE (Fig. 4, phase 1) was characterized by repeated periods of rainfall in a seasonal climate forced by precession in which chemical weathering (smectite formation) dominated the sedimentary signatures. This corresponds to maximum long eccentricity and shows the same climatic signature as during maximum eccentricity phases before the positive CIE. This is then followed by a second phase (Fig. 4, phase 2) where the climate is generally cooler and overall potentially more arid but with rainfall throughout the year over multiple precession cycles. This appears to have favoured deep physical erosion, owing to the abundance of primary clay minerals, kaolinite, and I-S R1. This interval corresponds to a minimum phase in the 405 kyr eccentricity based on Storm et al. (2020). This interpretation is further supported by decreasing and then low microcharcoal abundance, pointing to the suppression of fire activity at this time.

5.2.2 Climate forcing of sedimentary changes

Two coarsening-upward cycles that predate the onset of the positive CIE and continue for a few metres after its initiation are present in the detrital elemental ratios (best expressed in Si/Al and Zr/Rb records) (Figs. 3 and 4), and indicate a changing sediment influx over the studied interval. A previous study of the lithofacies of the Mochras borehole has also shown the coarsening-upward sequences of 0.5–3 m thickness, which are observed to be followed upwards by a thinner fining-upward succession (Pieńkowski et al., 2021). This reported fining-upward part is not reflected in the elemental ratios of the two sequences shown in this study. Furthermore, the coarsest phases of these sequences are approximately coeval with decreasing trends in the K/I ratio and increasing trends in S/I. This could indicate that periods of a strong monsoonal/seasonal climate (indicated by S/I) brought coarser-grained material to the basin, whereas periods of year-round humidity (K/I) are associated with higher chemical weathering (low Si/Al). Therefore, these two coarsening-upward cycles appear to link to increasing long eccentricity. A similar mechanism has been inferred for the northern South China Sea region in the Miocene, where coarser-grained material is found during periods of a strong summer monsoon and relatively lower chemical weathering (Clift et al., 2014). Present-day studies show that bedrock erosion and associated sediment transport is greater in areas with high seasonal contrast (Molnar, 2001, 2004). Hence, the Si/Al record also appears to reflect weathering and erosion conditions on land (Clift et al., 2014, 2020), driven by long-eccentricity-modulated climate (Fig. S5). However, other scenarios that would influence the grain size on this timescale cannot be dismissed and include changes in prox-

imity to siliciclastic sources or changes in sediment transport via bottom-water currents.

Changes in bottom-water current strength and direction likely affected the depositional site of the Mochras core (Pieńkowski et al., 2021) although there is as yet no consensus on the processes that likely controlled these palaeoceanographic parameters. In the UK region, the North Sea tectonic dome structure may have disrupted the circulation in the N–S Laurasian Seaway (including the Viking Corridor) in the late Pliensbachian when global sea levels are suggested to have been low (Haq, 2018) and therefore diminished the connectivity between the western Tethys and the Boreal realm, hypothetically reducing poleward heat transport from the tropics (Korte et al., 2015). This mechanism has also been argued to explain the later cooling observed in NW Europe during the transition of the warmer Toarcian to the cooler Aalenian and Bajocian (Korte et al., 2015). Late Pliensbachian occlusion of the Viking Corridor is supported by the provincialism of marine faunas at this time, showing a distinct Euro-Boreal province and a Mediterranean province (Dera et al., 2011). During the Toarcian, a northward expansion of invertebrate faunal species has been found (Schweigert, 2005; Zakharov et al., 2006; Bourillot et al., 2008; Nikitenko, 2008), indicating a northward (warmer) flow through the Viking Corridor (Korte et al., 2015). More recently, a southward expansion of Arctic dinoflagellates into the Viking Corridor was suggested for the termination of the T-OAE (Toarcian Oceanic Anoxic Event) (van de Schootbrugge et al., 2019), which is in agreement with a N to S flow through the Viking Corridor suggested by numerical models (Bjerrum et al., 2001; Dera and Donnadieu, 2012; Ruvalcaba Baroni et al., 2018) and sparse Nd isotopes (Dera et al., 2009).

Over the European epicontinental shelf (EES) and the Tethys as a whole, a clockwise circular gyre likely brought oxygenated warm Tethyan waters to the south-west shelf, with a progressively weaker north and eastward flow due to rough bathymetry and substantial island palaeo-geography (Ruvalcaba Baroni et al., 2018). This predominantly surface flow is modelled to have extended to shelfal sea floor depths. Only episodically might nutrient-rich boreal waters have penetrated south onto the EES in these coupled ocean–atmosphere general circulation model (GCM) scenarios (Dera and Donnadieu, 2012). The modelling also suggests – counter-intuitively – that the clockwise surface gyre of the Tethys extended further northwards and impacted the EES more effectively when the Hispanic Corridor was more open. The timing of the opening of the Hispanic Corridor is debated and varies from the Hettangian to Pliensbachian (Aberhan, 2001; Porter et al., 2013; Sha, 2019).

An alternative bottom current configuration was discussed for Mochras specifically, wherein changes in north-to-south current strength (see Bjerrum et al., 2001) are proposed for the changes in grain size and silt or sand versus clay content via contour currents (Pieńkowski et al., 2021). A strong flow from the cooler and shallow boreal waters is hypothesized

to have brought a coarser grain size fraction in suspension and as bedload, which was then deposited in the Cardigan Bay Basin while flowing to the deeper and warmer waters of the peri-Tethys (Pieńkowski et al., 2021). Times of a strong north-to-south current are proposed to be associated with more oxygenated bottom waters (Pieńkowski et al., 2021). In contrast, when the north-to-south current became weaker, less coarse material will have been carried in suspension and as bedload and a relatively higher clay proportion will have been deposited in the Cardigan Bay Basin (Pieńkowski et al., 2021). In this scenario, times of sluggish currents are associated with low bottom-water oxygenation (Pieńkowski et al., 2021) and thus climate forcing of current strength could explain the deposition of alternating coarser and finer fractions in the Mochras borehole (Pieńkowski et al., 2021).

Our research suggests that orbital cycles both before and during the onset of the positive CIE have a significant influence on seasonality and hydrology, affecting both fire regimes and sediment depositional character. Further research is required to consider how long eccentricity and obliquity cycles might interact with north–south flow in the Cardigan Bay Basin and circulation processes. What is clear is that orbital cycles have an impact on terrestrial processes in the terrestrial sediment source areas (Hollaar et al., 2021) and led to differences in deposition within the marine sediments in the Mochras core (Ruhl et al., 2016; Pieńkowski et al., 2021). Our data indicate that periods of coarser-sediment deposition correspond to periods that include more seasonal climates before the onset of the positive CIE (low kaolinite), which is in line with the hypothesized grain size changes caused by contour currents (Pieńkowski et al., 2021). However, after the onset of the positive CIE, although we suggest that the chemical weathering rate decreased, enhanced runoff and physical erosion are indicated by a peak in primary clay minerals and K/I. Enhanced runoff could be expected to impact the thermohaline contour currents (Dera and Donnadieu, 2012). Simultaneously, an increasingly cold climate (as indicated by enhanced physical erosion over chemical weathering) indicates a boreal influence. It remains to be determined to what extent orbital cycles might have the power to influence ocean circulation in the basin.

Relatively coarse sediments in the late Pliensbachian have also been related to shallower sediment deposition in UK basins (Hesselbo and Jenkyns, 1998; Hesselbo, 2008; Korte and Hesselbo, 2011). Around the UK area, these regressive facies are plausibly related to enhanced sediment shedding from the North Sea dome structure during sea level lowstand across the region (Korte and Hesselbo, 2011). Sequence stratigraphy of the Lower Jurassic of the Wessex, Cleveland, and Hebrides basins (Hesselbo and Jenkyns, 1998; Hesselbo, 2008; Archer et al., 2019) shows relative sea level changes and sand influxes in the late *Margaritatus* Zone in the studied basins. Noteworthy in the Mochras borehole are phases of low $\delta^{18}\text{O}$ of macrofossils which seem to correspond to high phases of macrofossil wood concomitant with

low sea level, suggesting a possible control of relative sea level on the oxygen-isotope record and the source of detrital material (Ullmann et al., 2022). The broad spatial distribution of these basins suggests that associated regression and/or sediment influx is of at least regional scale (Hesselbo, 2008). The results presented here fall within this phase of regression (Hesselbo and Jenkyns, 1998; Hesselbo, 2008).

In the context of the North Sea topographic dome structure (occlusion of the Viking Corridor in regional ocean flow) as a possible cause of the late Pliensbachian cooling, these facies can be interpreted as representing shallowing upward in relatively shallow water or the supply of coarser sediment into a deep-water system. The doming is hypothesized to have minimized or prohibited the southward flow of cooler waters from the Boreal and northward flow from warmer waters from the Mediterranean area (Korte et al., 2015). The Mochras borehole is situated on the south-western flank of the dome and would have been cut off from the northern parts of the Laurasian Seaway, including the Hebrides Basin and Cleveland Basin (Korte et al., 2015). This change in seaway circulation could have impacted the source area of the detrital sediments in the Mochras borehole.

Superimposed on these larger-scale factors affecting grain size, orbital forcing clearly also had a strong impact. The Cardigan Bay Basin (Mochras) is positioned about 290 km to the SW of the Cleveland Basin and at a similar latitude but to the west of the Wessex Basin (Ziegler, 1990; Torsvik and Cocks, 2017) and is therefore expected to be impacted by the same regional changes in sea level and/or sediment flux. In the late Pliensbachian of the Cleveland Basin, the detrital ratios of Si/Al, Zr/Al, and Zr/Rb show similar coarsening-upward sequences, which have been interpreted as reflecting changes in riverine transport of siliciclastic grains and grain size (Thibault et al., 2018). The inferred changes in sea level in the Cleveland Basin occur at a 100 kyr pacing (Huang and Hesselbo, 2014; Hesselbo et al., 2020b), potentially linking the regression cycles to short eccentricity (Huang et al., 2010, and references therein) and long eccentricity (Thibault et al., 2018). This would mean that eccentricity-driven changes in inferred sea level change could be linked to glacioeustatic cycles during these times (Brandt, 1986; Suan et al., 2010; Korte and Hesselbo, 2011; Krencker et al., 2019; Ruebsam et al., 2019, 2020b; Ruebsam and Schwark, 2021; Ruebsam and Al-Husseini, 2021). Glacioeustatic sea level changes are discussed for the Early Jurassic and Middle Jurassic (Krencker et al., 2019; Bodin et al., 2020; Ruebsam and Schwark, 2021; Nordt et al., 2022). A recent study on the rapid transgression observed at the Pliensbachian–Toarcian boundary ruled out other mechanisms that could force sea level at this timescale, such as aquifer eustasy, and emphasized that glacioeustatic changes in sea level are a likely possibility at times in the Early Jurassic (Krencker et al., 2019). Therefore, our findings overall are compatible with the episodic occurrence of continental ice at the poles (Brandt, 1986; Price, 1999; Suan et al., 2010; Korte and Hesselbo, 2011; Korte et al., 2015;

Bougeault et al., 2017; Krencker et al., 2019; Ruebsam et al., 2019, 2020a, b; Ruebsam and Schwark, 2021; Ruebsam and Al-Husseini, 2021).

6 Conclusions

The terrestrial environment adjacent to the Cardigan Bay Basin was strongly influenced by orbitally driven climate forcings (particularly precession and eccentricity) and colder climate linked to the Late Pliensbachian Event (LPE). Long-eccentricity forcing remained strong both prior to and during the LPE. Our results identify five swings in the climate in the study interval in tandem with the 405 kyr eccentricity minima and maxima. Eccentricity maxima are linked to precessionally repeated occurrences of a semi-arid monsoonal climate with high fire activity and relatively coarser sediment from terrestrial runoff. In contrast, 405 kyr minima in the Mochras core are linked to a more persistent, annually wet climate, low fire activity, and relatively finer-grained deposits across multiple precession cycles. Although the 405 kyr cycle in the proxy records persists through the onset of the LPE positive CIE, the expression in the clay mineralogical record changes to indicate year-round relatively cool and wet climate extended over multiple precession cycles driving significant erosion of bedrock. Therefore, both the Milankovitch forcings and larger climatic shifts operate in tandem to govern changes in the terrestrial environment.

Data availability. Supplementary data are available at the National Geoscience Data Centre at Keyworth (NGDC) at <https://doi.org/10.5285/1461dbe5-50a8-425c-8c49-ac1f04bcc271> (Hollaar, 2022) for the interval 934–918 m. b.s. All data presented for the interval 951–934 m. b.s. are available at the National Geoscience Data Centre at Keyworth (NGDC) at <https://doi.org/10.5285/d6b7c567-49f0-44c7-a94c-e82fa17ff98e> (Hollaar et al., 2021b). The full Mochras XRF dataset is in Damaschke et al. (2021) (<https://doi.org/10.5285/c09e9908-6a21-43a8-bc5a-944f9eb8b97e>).

Supplement. The supplement related to this article is available online at: <https://doi.org/10.5194/cp-19-979-2023-supplement>.

Author contributions. CMB, SPH, and TPH designed the research. TPH conducted the laboratory measurements, with JFD contributing to the XRD measurements and MD, CVU, and MJ to the XRF measurements. TPH, CMB, and SPH wrote the paper, with contributions from all authors.

Competing interests. The contact author has declared that none of the authors has any competing interests.

Disclaimer. Publisher's note: Copernicus Publications remains neutral with regard to jurisdictional claims in published maps and institutional affiliations.

Acknowledgements. This is a contribution to the JET project funded by the Natural Environment Research Council (NERC) (grant number NE/N018508/1). Stephen P. Hesselbo, Claire M. Belcher, Jean-François Deconinck, Clemens V. Ullmann, Mengjie Jiang, and Teuntje P. Hollaar, acknowledge funding from the International Continental Scientific Drilling Program (ICDP) and TPH acknowledges funding from the University of Exeter. We thank the British Geological Survey (BGS), especially James Riding and Scott Renshaw, for facilitating access to the Mochras core. We also thank Simon Wylde and Charles Gowing for their contribution to the XRF scanning and discussion of the results. We further thank Chris Mitchell for help with the TOC and $\delta^{13}\text{C}_{\text{org}}$ analyses. Finally, we thank Ludovic Bruneau for technical assistance with the XRD analysis. We thank referees Stéphane Bodin and Wolfgang Ruebsam for their very helpful comments and Mathieu Martinez for informal discussion.

Financial support. This research has been supported by the Natural Environment Research Council (grant no. NE/N018508/1) and the University of Exeter.

Review statement. This paper was edited by Luc Beaufort and reviewed by Stéphane Bodin and Wolfgang Ruebsam.

References

- Aberhan, M.: Bivalve palaeobiogeography and the Hispanic Corridor: time of opening and effectiveness of a proto-Atlantic seaway, *Palaeogeogr. Palaeoclimatol.*, 165, 375–394, [https://doi.org/10.1016/S0031-0182\(00\)00172-3](https://doi.org/10.1016/S0031-0182(00)00172-3), 2001.
- Alberti, M., Fürsich, F. T., and Andersen, N.: First steps in reconstructing Early Jurassic sea water temperatures in the Andean Basin of northern Chile based on stable isotope analyses of oyster and brachiopod shells, *J. Palaeogeogr.*, 8, 1–17, <https://doi.org/10.1186/s42501-019-0048-0>, 2019.
- Alberti, M., Parent, H., Garrido, A. C., Andersen, N., Garbe-Schönberg, D., and Danise, S.: Stable isotopes ($\delta^{13}\text{C}$, $\delta^{18}\text{O}$) and element ratios (Mg/Ca, Sr/Ca) of Jurassic belemnites, bivalves and brachiopods from the Neuquén Basin (Argentina): challenges and opportunities for palaeoenvironmental reconstructions, *J. Geol. Soc.*, 178, jgs2020-163, <https://doi.org/10.1144/jgs2020-163>, 2021.
- Archer, S. G., Steel, R. J., Mellere, D., Blackwood, S., and Cullen, B.: Response of Middle Jurassic shallow-marine environments to syn-depositional block tilting: Isles of Skye and Raasay, NW Scotland, *Scot. J. Geol.*, 55, 35–68, <https://doi.org/10.1144/sjg2018-014>, 2019.
- Bailey, T. R., Rosenthal, Y., McArthur, J. M., Van de Schootbrugge, B., and Thirlwall, M. F.: Paleooceanographic changes of the Late Pliensbachian–Early Toarcian interval: a possible link to the genesis of an Oceanic Anoxic Event, *Earth Planet. Sc. Lett.*,

- 212, 307–320, [https://doi.org/10.1016/S0012-821X\(03\)00278-4](https://doi.org/10.1016/S0012-821X(03)00278-4), 2003.
- Belcher, C. M., Collinson, M. E., and Scott, A. C.: Constraints on the thermal energy released from the Chicxulub impactor: new evidence from multi-method charcoal analysis, *J. Geol. Soc.*, 162, 591–602, <https://doi.org/10.1144/0016-764904-104>, 2005.
- Bjerrum, C. J., Surlyk, F., Callomon, J. H., and Slingerland, R. L.: Numerical paleoceanographic study of the Early Jurassic transcontinental Laurasian Seaway, *Paleoceanography*, 16, 390–404, <https://doi.org/10.1029/2000PA000512>, 2001.
- Bodin, S., Mau, M., Sadki, D., Danisch, J., Nutz, A., Krencker, F. N., and Kabiri, L.: Transient and secular changes in global carbon cycling during the early Bajocian event: Evidence for Jurassic cool climate episodes, *Global Planet. Change*, 194, 103287, <https://doi.org/10.1016/j.gloplacha.2020.103287>, 2020.
- Bodin, S., Fantasia, A., Krencker, F. N., Nebsbjerg, B., Christiansen, L., and Andrieu, S.: More gaps than record! A new look at the Pliensbachian/Toarcian boundary event guided by coupled chemo-sequence stratigraphy, *Palaeogeogr. Palaeoclimatol.*, 610, 111344, <https://doi.org/10.1016/j.palaeo.2022.111344>, 2023.
- Bougeault, C., Pellenard, P., Deconinck, J. F., Hesselbo, S. P., Dommergues, J. L., Bruneau, L., Cocquerez, T., Laffont, R., Huret, E., and Thibault, N.: Climatic and palaeoceanographic changes during the Pliensbachian (Early Jurassic) inferred from clay mineralogy and stable isotope (CO) geochemistry (NW Europe), *Global Planet. Change*, 149, 139–152, <https://doi.org/10.1016/j.gloplacha.2017.01.005>, 2017.
- Bourillot, R., Neige, P., Pierre, A., and Durllet, C.: Early–middle Jurassic Lytoceratid ammonites with constrictions from Morocco: palaeobiogeographical and evolutionary implications, *Palaeontology*, 51, 597–609, <https://doi.org/10.1111/j.1475-4983.2008.00766.x>, 2008.
- Brandt, K.: Glacioeustatic cycles in the Early Jurassic?, *Neues Jahrbuch für Geologie und Paläontologie-Monatshefte*, Schweizerbart Science Publishers, 257–274, <https://doi.org/10.1127/njgpm/1986/1986/257>, 1986.
- Calvert, S. E. and Pedersen, T. F.: Chapter fourteen elemental proxies for palaeoclimatic and palaeoceanographic variability in marine sediments: interpretation and application, *Dev. Mar. Geol.*, 1, 567–644, [https://doi.org/10.1016/S1572-5480\(07\)01019-6](https://doi.org/10.1016/S1572-5480(07)01019-6), 2007.
- Chamley, H.: *Clay Sedimentology*, Springer Verlag, Berlin, 623 pp., ISBN 978-3-642-85918-8, 1989.
- Chen, J., An, Z., and Head, J.: Variation of Rb/Sr ratios in the loess-paleosol sequences of central China during the last 130,000 years and their implications for monsoon paleoclimatology, *Quatern. Res.*, 51, 215–219, <https://doi.org/10.1006/qres.1999.2038>, 1999.
- Chen, J., Chen, Y., Liu, L., Ji, J., Balsam, W., Sun, Y., and Lu, H.: Zr/Rb ratio in the Chinese loess sequences and its implication for changes in the East Asian winter monsoon strength, *Geochim. Cosmochim. Acta.*, 70, 1471–1482, <https://doi.org/10.1016/j.gca.2005.11.029>, 2006.
- Cifer, T., Goričan, Š., Auer, M., Demény, A., Fraguas, Á., Gawlick, H. J., and Riechelmann, S.: Integrated stratigraphy (radiolarians, calcareous nannofossils, carbon and strontium isotopes) of the Sinemurian–Pliensbachian transition at Mt. Rettenstein, Northern Calcareous Alps, Austria, *Global Planet. Change*, 212, 103811, <https://doi.org/10.1016/j.gloplacha.2022.103811>, 2022.
- Clift, P. D., Wan, S., and Blusztajn, J.: Reconstructing chemical weathering, physical erosion and monsoon intensity since 25 Ma in the northern South China Sea: a review of competing proxies, *Earth Sci. Rev.*, 130, 86–102, <https://doi.org/10.1016/j.earscirev.2014.01.002>, 2014.
- Clift, P. D., Kulhanek, D. K., Zhou, P., Bowen, M. G., Vincent, S. M., Lyle, M., and Hahn, A.: Chemical weathering and erosion responses to changing monsoon climate in the Late Miocene of Southwest Asia, *Geol. Mag.*, 157, 939–955, <https://doi.org/10.1017/S0016756819000608>, 2020.
- Cobianchi, M. and Picotti, V.: Sedimentary and biological response to sea-level and palaeoceanographic changes of a Lower–Middle Jurassic Tethyan platform margin (Southern Alps, Italy), *Palaeogeogr. Palaeoclimatol.*, 169, 219–244, [https://doi.org/10.1016/S0031-0182\(01\)00217-6](https://doi.org/10.1016/S0031-0182(01)00217-6), 2021.
- Copetake, P. and Johnson, B.: Lower Jurassic Foraminifera from the Llanbedr (Mochras Farm) Borehole, North Wales, UK, *Monogr. Palaeontogr. Soc.*, 167, 1–403, 2014.
- Damaschke, M., Wylde, S., Jiang, M., Hollaar, T., and Ullmann, C. V.: Llanbedr (Mochras Farm) Core Scanning Dataset, NERC EDS National Geoscience Data Centre [data set], <https://doi.org/10.5285/c09e9908-6a21-43a8-bc5a-944f9eb8b97e>, 2021.
- Damborenea, S. E., Echevarria, J., and Ros-Franch, S.: Southern Hemisphere Palaeobiogeography of Triassic–Jurassic Marine Bivalves, Springer Briefs Seaways and Landbridges: Southern Hemisphere Biogeographic Connections Through Time, Springer Science and Business Media, Berlin, https://doi.org/10.1007/978-94-007-5098-2_1, 2013.
- Daniau, A. L., Sánchez Goñi, M. F., Martinez, P., Urrego, D. H., Bout-Roumazielle, V., Desprat, S., and Marlon, J. R.: Orbital-scale climate forcing of grassland burning in southern Africa, *P. Natl. Acad. Sci. USA*, 110, 5069–5073, <https://doi.org/10.1073/pnas.1214292110>, 2013.
- Deconinck, J. F., Hesselbo, S. P., and Pellenard, P.: Climatic and sea-level control of Jurassic (Pliensbachian) clay mineral sedimentation in the Cardigan Bay Basin, Llanbedr (Mochras Farm) borehole, Wales, *Sedimentology*, 66, 2769–2783, <https://doi.org/10.1111/sed.12610>, 2019.
- de Graciansky, P. C., Jacquin, T., and Hesselbo, S. P. (Eds.): *The Ligurian cycle: An overview of Lower Jurassic 2nd-order transgressive-regressive facies cycles in western Europe, Mesozoic and Cenozoic Sequence Stratigraphy of European Basins*, SEPM special publication 60, SEPM, 467–479, ISBN 1-565776-043-3, 1998.
- De Lena, L. F., Taylor, D., Guex, J., Bartolini, A., Adatte, T., van Acken, D., Spangenberg, J. E., Samankassou, E., Venne-mann, T., and Schaltegger, U.: The driving mechanisms of the carbon cycle perturbations in the late Pliensbachian (Early Jurassic), *Sci. Rep.-UK*, 9, 1–12, <https://doi.org/10.1038/s41598-019-54593-1>, 2019.
- Dera, G. and Donnadieu, Y.: Modeling evidences for global warming, Arctic seawater freshening, and sluggish oceanic circulation during the Early Toarcian anoxic event, *Paleoceanography*, 27, PA2211, <https://doi.org/10.1029/2012PA002283>, 2012.
- Dera, G., Pucéat, E., Pellenard, P., Neige, P., Delsate, D., Joachimski, M. M., Reisberg, L., and Martinez, M.: Water mass exchange and variations in seawater temperature in the NW Tethys during the Early Jurassic: evidence from neodymium and oxygen iso-

- topes of fish teeth and belemnites, *Earth Planet. Sc. Lett.*, 286, 198–207, <https://doi.org/10.1016/j.epsl.2009.06.027>, 2009.
- Dera, G., Neige, P., Dommergues, J. L., and Brayard, A.: Ammonite paleobiogeography during the Pliensbachian–Toarcian crisis (Early Jurassic) reflecting paleoclimate, eustasy, and extinctions, *Global Planet. Change*, 78, 92–105, <https://doi.org/10.1016/j.gloplacha.2011.05.009>, 2011.
- Dobson, M. R. and Whittington, R. J.: The geology of Cardigan Bay, *P. Geologist. Assoc.*, 98, 331–353, [https://doi.org/10.1016/S0016-7878\(87\)80074-3](https://doi.org/10.1016/S0016-7878(87)80074-3), 1987.
- Franceschi, M., Dal Corso, J., Posenato, R., Roghi, G., Masetti, D., and Jenkyns, H. C.: Early Pliensbachian (Early Jurassic) C-isotope perturbation and the diffusion of the Lithiotis Fauna: insights from the western Tethys, *Palaeogeogr. Palaeoclimatol.*, 410, 255–263, <https://doi.org/10.1016/j.palaeo.2014.05.025>, 2014.
- Gómez, J. J., Comas-Rengifo, M. J., and Goy, A.: Palaeoclimatic oscillations in the Pliensbachian (Early Jurassic) of the Asturian Basin (Northern Spain), *Clim. Past*, 12, 1199–1214, <https://doi.org/10.5194/cp-12-1199-2016>, 2016.
- Hallam, A.: A revised sea-level curve for the early Jurassic, *J. Geol. Soc.*, 138, 735–743, <https://doi.org/10.1144/gsjgs.138.6.0735>, 1981.
- Haq, B. U.: Jurassic sea-level variations: a reappraisal, *GSA Today*, 28, 4–10, 2018.
- Hesselbo, S. P.: Sequence stratigraphy and inferred relative sea-level change from the onshore British Jurassic, *P. Geologist. Assoc.*, 119, 19–34, [https://doi.org/10.1016/S0016-7878\(59\)80069-9](https://doi.org/10.1016/S0016-7878(59)80069-9), 2008.
- Hesselbo, S. P. and Jenkyns, H. C. (Eds.): British Lower Jurassic sequence stratigraphy, *Mesozoic and Cenozoic Sequence Stratigraphy of European Basins*, SEPM special publication 60, SEPM, 561–581, ISBN 1-565776-043-3, 1998.
- Hesselbo, S. P., Bjerrum, C. J., Hinnov, L. A., MacNiocaill, C., Miller, K. G., Riding, J. B., van de Schootbrugge, B., and the Mochras Revisited Science Team: Mochras borehole revisited: a new global standard for Early Jurassic earth history, *Sci. Drill.*, 16, 81–91, <https://doi.org/10.5194/sd-16-81-2013>, 2013.
- Hesselbo, S. P., Ogg, J. G., Ruhl, M., Hinnov, L. A., and Huang, C. J.: The Jurassic Period, in: *Geological Time Scale 2020*, edited by: Gradstein, F. M., Ogg, J. G., Schmitz, M. D., and Ogg, G. M., Elsevier, 955–1021, <https://doi.org/10.1016/B978-0-12-824360-2.00026-7>, 2020a.
- Hesselbo, S. P., Hudson, A. J. L., Huggett, J. M., Leng, M. J., Riding, J. B., and Ullmann, C. V.: Palynological, geochemical, and mineralogical characteristics of the Early Jurassic Liasidium Event in the Cleveland Basin, Yorkshire, UK, *Newsl. Stratigr.*, 53, 191–211, <https://doi.org/10.1127/nos/2019/0536>, 2020b.
- Hinnov, L. A., Ruhl, M., and Hesselbo, S. P.: Reply to the Comment on “Astronomical constraints on the duration of the Early Jurassic Pliensbachian Stage and global climatic fluctuations” [*Earth Planet. Sc. Lett.* 455 (2016) 149–165], *Earth Planet. Sc. Lett.*, 481, 415–419, <https://doi.org/10.1016/j.epsl.2016.08.038>, 2018.
- Hollaar, T.: Terrestrial palaeo-environmental proxy data of the Upper Pliensbachian, Mochras Borehole sediments, deposited in the Cardigan Bay Basin, Wales, NERC EDS National Geoscience Data Centre [data set] <https://doi.org/10.5285/d6b7c567-49f0-44c7-a94c-e82fa17ff98e>, 2021.
- Hollaar, T. P.: Palynofacies, microcharcoal, clay mineralogical and carbon isotope mass spectrometry measurements from the Late Pliensbachian (934–918 mbs) of the Mochras core, Cardigan Bay Basin, NW Wales, UK, NERC EDS National Geoscience Data Centre [data set], <https://doi.org/10.5285/1461dbe5-50a8-425c-8c49-ac1f04bcc271>, 2022.
- Hollaar, T. P., Baker, S. J., Hesselbo, S. P., Deconinck, J. F., Mander, L., Ruhl, M., and Belcher, C. M.: Wildfire activity enhanced during phases of maximum orbital eccentricity and precessional forcing in the Early Jurassic, *Commun. Earth Environ.*, 2, 1–12, <https://doi.org/10.1038/s43247-021-00307-3>, 2021.
- Huang, C. and Hesselbo, S. P.: Pacing of the Toarcian Oceanic Anoxic Event (Early Jurassic) from astronomical correlation of marine sections, *Gondwana Res.*, 25, 1348–1356, <https://doi.org/10.1016/j.gr.2013.06.023>, 2014.
- Huang, C., Hesselbo, S. P., and Hinnov, L.: Astrochronology of the late Jurassic Kimmeridge Clay (Dorset, England) and implications for Earth system processes, *Earth Planet. Sc. Lett.*, 289, 242–255, <https://doi.org/10.1016/j.epsl.2009.11.013>, 2010.
- Ilyina, V. I.: Jurassic palynology of Siberia, *Transactions of the Institute of Geology and Geophysics, Academy of Sciences of the USSR, Siberian Branch*, 638, Nauka Publishing House, Moscow, p. 237, <https://www.geokniga.org/books/11830> (last access: 5 May 2023), 1985.
- Ivimey-Cook, H. C.: Stratigraphical palaeontology of the Lower Jurassic of the Llanbedr (Mochras Farm) Borehole, in: *The Llanbedr (Mochras Farm) Borehole*, edited by: Woodland, A. W., Rep. No. 71/18, Institute of Geological Sciences, 87–92, 1971.
- Jenkyns, H. C. and Clayton, C. J.: Black shales and carbon isotopes in pelagic sediments from the Tethyan Lower Jurassic, *Sedimentology*, 33, 87–106, <https://doi.org/10.1111/j.1365-3091.1986.tb00746.x>, 1986.
- Kaplan, M. E.: Calcite pseudomorphoses in Jurassic and Lower Cretaceous deposits of the northern area of eastern Siberia, *Geologiya i Geofizika*, 19, 62–70, 1978.
- Korte, C. and Hesselbo, S. P.: Shallow-marine carbon- and oxygen-isotope and elemental records indicate icehouse-greenhouse cycles during the Early Jurassic, *Paleoceanography*, 26, PA4219, <https://doi.org/10.1029/2011PA002160>, 2011.
- Korte, C., Hesselbo, S. P., Ullmann, C. V., Dietl, G., Ruhl, M., Schweigert, G., and Thibault, N.: Jurassic climate mode governed by ocean gateway, *Nat. Commun.*, 6, 1–7, <https://doi.org/10.1038/ncomms10015>, 2015.
- Krencker, F. N., Lindström, S., and Bodin, S.: A major sea-level drop briefly precedes the Toarcian oceanic anoxic event: implication for Early Jurassic climate and carbon cycle, *Sci. Rep.-UK*, 9, 1–12, <https://doi.org/10.1038/s41598-019-48956-x>, 2019.
- Krencker, F. N., Fantasia, A., Danisch, J., Martindale, R., Kabiri, L., El Ouali, M., and Bodin, S.: Two-phased collapse of the shallow-water carbonate factory during the late Pliensbachian–Toarcian driven by changing climate and enhanced continental weathering in the Northwestern Gondwana Margin, *Earth-Sci. Rev.*, 208, 103254, <https://doi.org/10.1016/j.earscirev.2020.103254>, 2020.
- Laskar, J.: Astrochronology, in: *Geological Time Scale*, edited by: Gradstein, F. M., Ogg, J. G., and Ogg, G. M., Elsevier, 139–158, <https://doi.org/10.1016/B978-0-12-824360-2.00004-8>, 2020.
- Laskar, J., Fienga, A., Gastineau, M., and Manche, H.: La2010: a new orbital solution for the long-term motion of the Earth, *Astron. Astrophys.*, 532, A89, <https://doi.org/10.1051/0004-6361/201116836>, 2011.

- Martinez, M. and Dera, G.: Orbital pacing of carbon fluxes by a ~ 9 -My eccentricity cycle during the Mesozoic, *P. Natl. Acad. Sci. USA*, 112, 12604–12609, <https://doi.org/10.1073/pnas.1419946112>, 2015.
- McArthur, J. M., Donovan, D. T., Thirlwall, M. F., Fouke, B. W., and Matthey, D.: Strontium isotope profile of the early Toarcian (Jurassic) oceanic anoxic event, the duration of ammonite biozones, and belemnite palaeotemperatures, *Earth Planet. Sc. Lett.*, 179, 269–285, [https://doi.org/10.1016/S0012-821X\(00\)00111-4](https://doi.org/10.1016/S0012-821X(00)00111-4), 2000.
- McElwain, J. C., Wade-Murphy, J., and Hesselbo, S. P.: Changes in carbon dioxide during an oceanic anoxic event linked to intrusion into Gondwana coals, *Nature*, 435, 479–482, <https://doi.org/10.1038/nature03618>, 2005.
- Mercuzot, M., Pellenard, P., Durllet, C., Bougeault, C., Meister, C., Dommergues, J. L., Thibault, N., Baudin, F., Mathieu, O., Bruneau, L., Huret, E., and El Hmidi, K.: Carbon-isotope events during the Pliensbachian (Lower Jurassic) on the African and European margins of the NW Tethyan Realm, *Newsl. Stratigr.*, 53, 41–69, <https://doi.org/10.1127/nos/2019/0502>, 2020.
- Merriman, R. J.: Clay mineral assemblages in British Lower Palaeozoic mudrocks, *Clay Miner.*, 41, 473–512, <https://doi.org/10.1180/0009855064110204>, 2006.
- Moiroud, M., Martinez, M., Deconinck, J.F., Monna, F., Pellenard, P., Riquier, L., and Company, M.: High-resolution clay mineralogy as a proxy for orbital tuning: example of the Hauterivian–Barremian transition in the Betic Cordillera (SE Spain), *Sediment. Geol.*, 282, 336–346, <https://doi.org/10.1016/j.sedgeo.2012.10.004>, 2012.
- Molnar, P.: Climate change, flooding in arid environments, and erosion rates, *Geology*, 29, 1071–1074, [https://doi.org/10.1130/0091-7613\(2001\)029<1071:CCFIAE>2.0.CO;2](https://doi.org/10.1130/0091-7613(2001)029<1071:CCFIAE>2.0.CO;2), 2001.
- Molnar, P.: Late Cenozoic increase in accumulation rates of terrestrial sediment: How might climate change have affected erosion rates?, *Annu. Rev. Earth Planet. Sci.*, 32, 67–89, <https://doi.org/10.1146/annurev.earth.32.091003.143456>, 2004.
- Moore, D. M. and Reynolds, R. C.: X-Ray Diffraction and the Identification and Analysis of Clay Minerals, Oxford University Press, New York, 378 pp., ISBN 0195087135, 1997.
- Morettini, E., Santantonio, M., Bartolini, A., Cecca, F., Baumgartner, P. O., and Hunziker, J. C.: Carbon isotope stratigraphy and carbonate production during the Early–Middle Jurassic: examples from the Umbria–Marche–Sabina Apennines (central Italy), *Palaeogeogr. Palaeoclimatol.*, 184, 251–273, [https://doi.org/10.1016/S0031-0182\(02\)00258-4](https://doi.org/10.1016/S0031-0182(02)00258-4), 2002.
- Munier, T., Deconinck, J. F., Pellenard, P., Hesselbo, S. P., Riding, J. B., Ullmann, C. V., Bougeault, C., Mercuzot, M., Santoni, A. L., Huret, É., and Landrein, P.: Million-year-scale alternation of warm–humid and semi-arid periods as a mid-latitude climate mode in the Early Jurassic (late Sinemurian, Laurasian Seaway), *Clim. Past*, 17, 1547–1566, <https://doi.org/10.5194/cp-17-1547-2021>, 2021.
- Nikitenko, B. L.: The Early Jurassic to Aalenian paleobiogeography of the Arctic Realm: implication of microbenthos (Foraminifers and Ostracodes), *Stratigr. Geol. Correl.*, 16, 59–80, <https://doi.org/10.1007/s11506-008-1005-z>, 2008.
- Nordt, L., Breecker, D., and White, J.: Jurassic greenhouse ice-sheet fluctuations sensitive to atmospheric CO₂ dynamics, *Nat. Geosci.*, 15, 54–59, <https://doi.org/10.1038/s41561-021-00858-2>, 2022.
- Oboh-Ikuenobe, F. E., Obi, C. G., and Jaramillo, C. A.: Lithofacies, palynofacies, and sequence stratigraphy of Palaeogene strata in Southeastern Nigeria, *J. Afr. Earth Sci.*, 41, 79–101, <https://doi.org/10.1016/j.jafrearsci.2005.02.002>, 2005.
- Petschick, R.: MacDiff 4.2.2, <http://servermac.geologie.unfrankfurt.de/Rainer.html> (last access: 9 February 2020), 2000.
- Pieńkowski, G., Uchman, A., Ninard, K., and Hesselbo, S. P.: Ichthyology, sedimentology, and orbital cycles in the hemipelagic Early Jurassic Laurasian Seaway (Pliensbachian, Cardigan Bay Basin, UK), *Global Planet. Change*, 207, 103648, <https://doi.org/10.1016/j.gloplacha.2021.103648>, 2021.
- Porter, S. J., Selby, D., Suzuki, K., and Gröcke, D.: Opening of a trans-Pangaeian marine corridor during the Early Jurassic: Insights from osmium isotopes across the Sinemurian–Pliensbachian GSSP, Robin Hood’s Bay, UK, *Palaeogeogr. Palaeoclimatol.*, 375, 50–58, <https://doi.org/10.1016/j.palaeo.2013.02.012>, 2013.
- Price, G. D.: The evidence and implications of polar ice during the Mesozoic, *Earth-Sci. Rev.*, 48, 183–210, [https://doi.org/10.1016/S0012-8252\(99\)00048-3](https://doi.org/10.1016/S0012-8252(99)00048-3), 1999.
- Price, G. D., Baker, S. J., Van De Velde, J., and Clémence, M. E.: High-resolution carbon cycle and seawater temperature evolution during the Early Jurassic (Sinemurian–Early Pliensbachian), *Geochem. Geophys. Geosyst.*, 17, 3917–3928, <https://doi.org/10.1002/2016GC006541>, 2016.
- Quesada, S., Robles, S., and Rosales, I.: Depositional architecture and transgressive–regressive cycles within Liassic backstepping carbonate ramps in the Basque–Cantabrian Basin, northern Spain, *J. Geol. Soc.*, 162, 531–548, <https://doi.org/10.1144/0016-764903-041>, 2005.
- Raucsik, B. and Varga, A.: Climato-environmental controls on clay mineralogy of the Hettangian–Bajocian successions of the Mecsek Mountains, Hungary: an evidence for extreme continental weathering during the early Toarcian oceanic anoxic event, *Palaeogeogr. Palaeoclimatol.*, 265, 1–13, <https://doi.org/10.1016/j.palaeo.2008.02.004>, 2008.
- Riding, J. B., Leng, M. J., Kender, S., Hesselbo, S. P., and Feist-Burkhardt, S.: Isotopic and palynological evidence for a new Early Jurassic environmental perturbation, *Palaeogeogr. Palaeoclimatol.*, 374, 16–27, <https://doi.org/10.1016/j.palaeo.2012.10.019>, 2013.
- Robinson, S. A., Ruhl, M., Astley, D. L., Naafs, B. D. A., Farnsworth, A. J., Bown, P. R., Hugh, J. C., Lunt, D. J., O’Brien, C., Pancost, R. D., and Markwick, P. J.: Early Jurassic North Atlantic sea-surface temperatures from TEX 86 palaeothermometry, *Sedimentology*, 64, 215–230, <https://doi.org/10.1111/sed.12321>, 2016.
- Rogov, M. A. and Zakharov, V. A.: Jurassic and Lower Cretaceous glendonite occurrences and their implication for Arctic paleoclimate reconstructions and stratigraphy, *Earth Sci. Front.*, 17, 345–347, 2010.
- Rosales, I., Quesada, S., and Robles, S.: Paleotemperature variations of Early Jurassic seawater recorded in geochemical trends of belemnites from the Basque–Cantabrian basin, northern Spain, *Palaeogeogr. Palaeoclimatol.*, 203, 253–275, [https://doi.org/10.1016/S0031-0182\(03\)00686-2](https://doi.org/10.1016/S0031-0182(03)00686-2), 2004.

- Rosales, I., Quesada, S., and Robles, S.: Geochemical arguments for identifying second-order sea-level changes in hemipelagic carbonate ramp deposits, *Terra Nova*, 18, 233–240, <https://doi.org/10.1111/j.1365-3121.2006.00684.x>, 2006.
- Ruebsam, W. and Al-Husseini, M.: Orbitally synchronized late Pliensbachian–early Toarcian glacio-eustatic and carbon-isotope cycles, *Palaeogeogr. Palaeoclimatol., 577*, 110562, <https://doi.org/10.1016/j.palaeo.2021.110562>, 2021.
- Ruebsam, W. and Schwark, L.: Impact of a northern-hemispherical cryosphere on late Pliensbachian–early Toarcian climate and environment evolution, *Geol. Soc. Spec. Publ. Lond.*, 514, 359–385, <https://doi.org/10.1144/SP514-2021-11>, 2021.
- Ruebsam, W., Mayer, B., and Schwark, L.: Cryosphere carbon dynamics control early Toarcian global warming and sea level evolution, *Global Planet. Change*, 172, 440–453, <https://doi.org/10.1016/j.gloplacha.2018.11.003>, 2019.
- Ruebsam, W., Reolid, M., Sabatino, N., Masetti, D., and Schwark, L.: Molecular paleothermometry of the early Toarcian climate perturbation, *Global Planet. Change*, 195, 103351, <https://doi.org/10.1016/j.gloplacha.2020.103351>, 2020a.
- Ruebsam, W., Thibault, N., and Al-Husseini, M.: Early Toarcian glacio-eustatic unconformities and chemostratigraphic black holes, in: *Stratigraphy and Timescales*, edited by: Montenari, M., Academic Press, 629–676, <https://doi.org/10.1016/bs.sats.2020.08.006>, 2020b.
- Ruffell, A., McKinley, J. M., and Worden, R. H.: Comparison of clay mineral stratigraphy to other proxy palaeoclimate indicators in the Mesozoic of NW Europe, *Philos. T. Roy. Soc. A*, 360, 675–693, <https://doi.org/10.1098/rsta.2001.0961>, 2002.
- Ruhl, M., Hesselbo, S. P., Hinnov, L., Jenkyns, H. C., Xu, W., Riding, J. B., Storm, M., Minisini, D., Ullmann, C. V., and Leng, M. J.: Astronomical constraints on the duration of the Early Jurassic Pliensbachian Stage and global climatic fluctuations, *Earth Planet. Sc. Lett.*, 455, 149–165, <https://doi.org/10.1016/j.epsl.2016.08.038>, 2016.
- Ruvalcaba Baroni, I., Pohl, A., van Helmond, N. A., Papadomanolaki, N. M., Coe, A. L., Cohen, A. S., van de Schootbrugge, B., Donnadiou, Y., and Slomp, C. P.: Ocean circulation in the Toarcian (Early Jurassic): a key control on deoxygenation and carbon burial on the European Shelf, *Paleoceanogr. Paleoclimatol.*, 33, 994–1012, <https://doi.org/10.1029/2018PA003394>, 2018.
- Schweigert, G.: The occurrence of the Tethyan ammonite genus *Meneghiniceras* (Phylloceratina: Juraphyllitidae) in the Upper Pliensbachian of SW Germany, *Stuttgarter Beiträge zur Naturkunde Serie B Geologie und Paläontologie*, 356, 1–15, 2005.
- Scott, A. C.: Charcoal recognition, taphonomy and uses in palaeoenvironmental analysis, *Palaeogeogr. Palaeoclimatol.*, 291, 11–39, <https://doi.org/10.1016/j.palaeo.2009.12.012>, 2010.
- Sellwood, B. W. and Jenkyns, H. G.: Basins and swells and the evolution of an epeiric sea: (Pliensbachian–Bajocian of Great Britain), *J. Geol. Soc.*, 131, 373–388, <https://doi.org/10.1144/gsjgs.131.4.0373>, 1975.
- Sha, J.: Opening time of the Hispanic Corridor and migration patterns of pan-tropical cosmopolitan Jurassic pectinid and ostreid bivalves, *Palaeogeogr. Palaeoclimatol.*, 515, 34–46, <https://doi.org/10.1016/j.palaeo.2018.09.018>, 2019.
- Silva, R. L., Duarte, L. V., Comas-Rengifo, M. J., Mendonça Filho, J. G., and Azerêdo, A. C.: Update of the carbon and oxygen isotopic records of the Early–Late Pliensbachian (Early Jurassic, ~ 187 Ma): Insights from the organic-rich hemipelagic series of the Lusitanian Basin (Portugal), *Chem. Geol.*, 283, 177–184, <https://doi.org/10.1016/j.chemgeo.2011.01.010>, 2011.
- Silva, R. L., Duarte, L. V., Wach, G. D., Ruhl, M., Sadki, D., Gómez, J. J., Hesselbo, S. P., Xu, W., O’Connor, D., Rodrigues, B., and Mendonça Filho, J. G.: An Early Jurassic (Sinemurian–Toarcian) stratigraphic framework for the occurrence of Organic Matter Preservation Intervals (OMPIs), *Earth Sci. Rev.*, 221, 103780, <https://doi.org/10.1016/j.earscirev.2021.103780>, 2021.
- Slater, S. M., Bown, P., Twitchett, R. J., Danise, S., and Vajda, V.: Global record of “ghost” nannofossils reveals plankton resilience to high CO₂ and warming, *Science*, 376, 853–856, <https://doi.org/10.1126/science.abm7330>, 2022.
- Smith, P. L.: The Pliensbachian ammonite *Dayiceras dayiceroides* and early Jurassic paleogeography, *Can. J. Earth Sci.*, 20, 86–91, <https://doi.org/10.1139/e83-008>, 1983.
- Steinthorsdottir, M. and Vajda, V.: Early Jurassic (late Pliensbachian) CO₂ concentrations based on stomatal analysis of fossil conifer leaves from eastern Australia, *Gondwana Res.*, 27, 932–939, <https://doi.org/10.1016/j.gr.2013.08.021>, 2015.
- Storm, M. S., Hesselbo, S. P., Jenkyns, H. C., Ruhl, M., Ullmann, C. V., Xu, W., Leng, M. J., Riding, J. B., and Gorbatenko, O.: Orbital pacing and secular evolution of the Early Jurassic carbon cycle, *P. Natl. Acad. Sci. USA*, 117, 3974–3982, <https://doi.org/10.1073/pnas.1912094117>, 2020.
- Suan, G., Mattioli, E., Pittet, B., Lécuyer, C., Suchéras-Marx, B., Duarte, L. V., Philippe, M., Reggiani, L., and Martineau, F.: Secular environmental precursors to Early Toarcian (Jurassic) extreme climate changes, *Earth Planet. Sc. Lett.*, 290, 448–458, <https://doi.org/10.1016/j.epsl.2009.12.047>, 2010.
- Suan, G., Nikitenko, B. L., Rogov, M. A., Baudin, F., Spangenberg, J. E., Knyazev, V. G., Glinskikh, L. A., Goryacheva, A. A., Adatte, T., Riding, J. B., Föllmi, K. B., Pittet, B., Mattioli, E., and Lécuyer, C.: Polar record of Early Jurassic massive carbon injection, *Earth Planet. Sc. Lett.*, 312, 102–113, <https://doi.org/10.1016/j.epsl.2011.09.050>, 2011.
- Tappin, D. R., Chadwick, R. A., Jackson, A. A., Wingfield, R. T. R., and Smith, N. J. P.: Geology of Cardigan Bay and the Bristol Channel, United Kingdom offshore regional report, British Geological Survey, HMSO, 107 pp., ISBN 0118845063, 1994.
- Thibault, N., Ruhl, M., Ullmann, C. V., Korte, C., Kemp, D. B., Gröcke, D. R., and Hesselbo, S. P.: The wider context of the Lower Jurassic Toarcian oceanic anoxic event in Yorkshire coastal outcrops, UK, *Proc. Geologist. Assoc.*, 129, 372–391, <https://doi.org/10.1016/j.pgeola.2017.10.007>, 2018.
- Thiry, M.: Palaeoclimatic interpretation of clay minerals in marine deposits: an outlook from the continental origin, *Earth-Sci. Rev.*, 49, 201–221, [https://doi.org/10.1016/S0012-8252\(99\)00054-9](https://doi.org/10.1016/S0012-8252(99)00054-9), 2000.
- Torsvik, T. H. and Cocks, L. R. M. (Eds.): *Jurassic*, in: *Earth History and Palaeogeography*, Cambridge University Press, 208–218, ISBN 1107105323, 2017.
- Ullmann, C. V., Szűcs, D., Jiang, M., Hudson, A. J., and Hesselbo, S. P.: Geochemistry of macrofossil, bulk rock, and secondary calcite in the Early Jurassic strata of the Llanbedr (Mochras Farm) drill core, Cardigan Bay Basin, Wales, UK, *J. Geol. Soc.*, 179, jgs2021-018, <https://doi.org/10.1144/jgs2021-018>, 2022.

- Underhill, J. R. and Partington, M. A.: Jurassic thermal doming and deflation in the North Sea: implications of the sequence stratigraphic evidence, *Petroleum Geology Conference series 4*, Geological Society, London, 337–345, <https://doi.org/10.1144/0040337>, 1993.
- van de Schootbrugge, B., Bailey, T. R., Rosenthal, Y., Katz, M. E., Wright, J. D., Miller, K. G., Feist-Burkhardt, S., and Falkowski, P. G.: Early Jurassic climate change and the radiation of organic-walled phytoplankton in the Tethys Ocean, *Paleobiology*, 31, 73–97, [https://doi.org/10.1666/0094-8373\(2005\)031<0073:EJCCAT>2.0.CO;2](https://doi.org/10.1666/0094-8373(2005)031<0073:EJCCAT>2.0.CO;2), 2005.
- van de Schootbrugge, B., Houben, A. J. P., Ercan, F. E. Z., Verreussel, R., Kerstholt, S., Janssen, N. M. M., Nikitenko, B., and Suan, G.: Enhanced arctic-tethys connectivity ended the toarcian oceanic anoxic event in NW Europe, *Geol. Mag.*, 157, 1593–1611, <https://doi.org/10.1017/S0016756819001262>, 2019.
- Waterhouse, H. K.: Orbital forcing of palynofacies in the Jurassic of France and the United Kingdom, *Geology*, 27, 511–514, [https://doi.org/10.1130/0091-7613\(1999\)027<0511:OFOPIT>2.3.CO;2](https://doi.org/10.1130/0091-7613(1999)027<0511:OFOPIT>2.3.CO;2), 1999.
- Weedon, G. P.: Hemipelagic shelf sedimentation and climatic cycles: the basal Jurassic (Blue Lias) of South Britain, *Earth Planet. Sc. Lett.*, 76, 321–335, [https://doi.org/10.1016/0012-821X\(86\)90083-X](https://doi.org/10.1016/0012-821X(86)90083-X), 1986.
- Weedon, G. P. and Jenkyns, H. C.: Regular and irregular climatic cycles and the Belemnite Marls (Pliensbachian, Lower Jurassic, Wessex Basin), *J. Geol. Soc.*, 147, 915–918, <https://doi.org/10.1144/gsjgs.147.6.0915>, 1990.
- Weedon, G. P., Page, K. N., and Jenkyns, H. C.: Cyclostratigraphy, stratigraphic gaps and the duration of the Hettangian Stage (Jurassic): insights from the Blue Lias Formation of southern Britain, *Geol. Mag.*, 156, 1469–1509, <https://doi.org/10.1017/S0016756818000808>, 2019.
- Woodland, A. W. (Ed.): *The Llanbedr (Mochras Farm) Borehole*, Report No. 71/18, Institute of Geological Sciences, London, 115 pp., 1971.
- Zakharov, V. A., Shurygin, B. N., Il'ina, V. I., and Nikitenko, B. L.: Pliensbachian-Toarcian biotic turnover in north Siberia and the Arctic region, *Stratigr. Geol. Correl.*, 14, 399–417, <https://doi.org/10.1134/S0869593806040046>, 2006.
- Ziegler, P. A.: *Geological Atlas of Western and Central Europe*, 239, Shell Internationale Petroleum Maatschappij, the Hague, 1990.